THERMAL MODELS AND MICROWAVE TEMPERATURES OF THE PLANET MERCURY

D. Morrison

Smithsonian Astrophysical Observatory
SPECIAL REPORT 292

Research in Space Science
SAO Special Report No. 292

THERMAL MODELS AND MICROWAVE TEMPERATURES OF THE PLANET MERCURY

David Morrison

January 31, 1969

Smithsonian Institution
Astrophysical Observatory
Cambridge, Massachusetts 02138

809-199

TABLE OF CONTENTS

TABLE OF CONTENTS (Cont.)

LIST OF ILLUSTRATIONS

LIST OF ILLUSTRATIONS (Cont.)

LIST OF ILLUSTRATIONS (Cont.)

ABSTRACT

Several physical properties of the epilith of Mercury can be investigated by a comparison of infrared and microwave brightness temperatures with the predictions of theoretical thermal models of the planet. The results presented here have been obtained by numerical solution of the one-dimensional heat-conduction equation with temperature-dependent thermal conductivity, using surface boundary conditions that include the modification of the insolation cycles by the spin-orbit coupling and large orbital eccentricity of the planet. For comparison with microwave observations, disk-averaged brightness temperatures are presented as a function of phase angle and heliocentric longitude of Mercury for wavelengths of 0.12, 0.34, 0.80, 1.90, 3.75, and 11.30 cm. These predictions are compared with calculations from simpler lunar-type models and are used to analyze the existing infrared and microwave observations of the planet. A means of determining observationally both the mean thermal parameter $(K\rho c)^{-1/2}$ cal^{-1} cm^2 $sec^{1/2}$ deg and the significance of an effective conductivity due to radiative thermal-energy transport is presented.

The observations of a microwave phase effect are all found to be compatible with a ratio of electrical to thermal skin depths approximately equal to the wavelength. The thermal parameter is, from infrared observations, larger than 200 cal^{-1} cm^2 $sec^{1/2}$ deg, indicating a thermal conductivity less than 10^{-4} cal cm^{-1} sec^{-1} deg. The loss tangent of the material is greater than 2×10^{-3}. Although some contradictions are present, the observations strongly suggest an increase of mean brightness temperature with wavelength, indicating a significant radiative contribution to the subsurface thermal conductivity. All these conclusions are consistent with the hypothesis that the epilith of Mercury is physically very similar to that of the Moon.

RÉSUMÉ

Plusieurs propriétés physiques de l'épilithe de Mercure peuvent être étudiées en comparant les températures de brilliance dans l'infrarouge et les ondes ultracourtes avec les prédictions théoriques des modèles thermiques de la planète. Les résultats présentés ici ont été obtenus par la solution numérique de l'équation unidimensionnelle de conduction de la chaleur, la conductivité thermique dépendant de la température; des conditions limites à la surface comprenant la modification des cycles d'insolation par le couplage spin-orbite et la grande excentricité orbitale de la planète ont été employées. Les moyennes des températures de brilliance obtenues sur le disque sont représentées en fonction de l'angle de phase et de la longitude héliocentrique de Mercure pour les longueurs d'onde 0,12, 0,34, 0,84, 1,90, 3,75, et 11,30 cm, afin de les comparer avec les observations faites avec les ondes ultracourtes. Ces prédictions sont comparées avec les calculs faits à partir de modèles plus simples du type lunaire et sont employées pour analyser les observations de la planète que l'on a dans l'infrarouge et les ondes ultracourtes. Nous présentons un moyen de déterminer par l'observation à la fois le paramètre thermique moyen $(K\rho c)^{-1/2}$ $cal^{-1}cm^{2}sec^{1/2}deg$ et l'importance d'une conductivité effective due au transport de l'énergie thermique radiative.

Nous trouvons que toutes les observations d'un effet de phase en ondes ultracourtes sont compatibles avec un rapport des profondeurs de peau électriques et thermiques approximativement égal à la longueur d'onde. A partir des observations dans l'infrarouge, nous déduisons que le paramètre thermique est plus grand que 200 $cal^{-1}cm^{2}sec^{1/2}deg$, ce qui indique une conductivité thermique inférieure à 10^{-4} cal $cm^{-1}deg$. La tangente de perte qui caractérise la matière est supérieure à 2.10^{-3}. Bien qu'il y ait certaines contradictions, les observations permettent de

penser qu'il y a un accroissement de la température de brillance moyenne avec les longueurs d'onde ce qui indique une importante contribution radiative à la conductivité thermique de la sous-surface. Toutes ces conclusions sont compatibles avec l'hypothèse que l'épilithe de Mercure est physiquement très semblable à celle de la lune.

КОНСПЕКТ

Несколько физических свойств эпилита Меркурия могут быть изучаемы путем сравнения инфракрасной и микроволновой температур яркости с предсказаниями теоретических тепловых моделей планеты. Приведенные здесь результаты были получены с помощью числового решения одно-размерного уравнения теплопроводности с зависящей от температуры теплопроводностью, пользуясь граничными условиями поверхности включающих изменение циклов инсоляции взаимодействием спин-орбиты и большим эксцентриситетом орбиты планеты. Для сравнения с микроволновыми наблюдениями, усередненные по диску температуры яркости приводятся как функции фазового угла и гелиоцентрической долготы Меркурия для длин волн в 0,12 0,34, 0,80, 1,90, 3,75 и 11,30 см. Эти прогнозы сравниваются с вычислениями для более простых лунного типа моделей и применяются для анализа имеющихся инфракрасных и микроволновых наблюдений планеты. Приводится способ определения, путем наблюдений, обоих среднего теплового параметра $(K\rho c)^{-1/2}$ кал$^{-1}$ см^{2} сек$^{1/2}$ град и значения эффективной проводности вызываемой переносом излучаемой тепловой энергии.

Все наблюдения микроволнового эффекта фазы были найдены согласными с соотношением между электрическими и температурными поверхностными глубинами приблизительно равными длине волны. Тепловой параметр является, исходя из инфракрасных наблюдений, больше чем 200 кал$^{-1}$ см^{2} сек$^{1/2}$ град, указывая на то что теплопроводность является менее 10^{-4} кал см$^{-1}$ сек$^{-1}$ град. Касательная

потеря материала является больше 2×10^{-3}. Несмотря на присутствие нескольких противоречий, наблюдения сильно намекают на рост средней температуры яркости с длиной волны, указывая на значительный вклад излучения в подповерхностную теплопроводность. Все эти заключения совместимы с гипотезой что эпилит Меркурия является физически очень сходным с лунным.

THERMAL MODELS AND MICROWAVE TEMPERATURES OF THE PLANET MERCURY

David Morrison

1. INTRODUCTION

The discovery by Pettengill and Dyce (1965) at Arecibo Observatory that Mercury is not in synchronous rotation has led to a period of renewed interest in the physical nature of the planet. The unexpectedly high microwave temperature observed near inferior conjunction at 3.75-cm wavelength by Howard, Barrett, and Haddock (1962) can now be understood. At the same time, observations of a microwave phase effect have been reported at several wavelengths, and infrared measurements of planetary surface temperature are also within present capabilities. This report attempts to apply simple models to the thermal behavior of Mercury and to use these together with the considerable body of available data to evaluate some physical properties of the planet. Partial results from this investigation have been presented by Morrison and Sagan (1967, 1968) and Morrison (1968a).

The radar observations (Dyce, Pettengill, and Shapiro, 1967) indicate that Mercury rotates in a direct sense with a sidereal period of 59 ± 3 days. Optical studies (McGovern, Gross, and Rasool, 1965; Chapman, 1967; Camichel and Dollfus, 1968; Smith and Reese, 1968) suggest that the rotation period is exactly 2/3 of the orbital period, or 58.646 days; this conclusion is also supported by studies of the stability of tidal locking (Colombo, 1965; Liu and O'Keefe, 1965; Colombo and Shapiro, 1966; Peale and Gold, 1965; Goldreich and Peale, 1968). With this rotation period, the solar day on Mercury is 176 days long, equal to two orbital revolutions and to three

This work was supported in part by grant NGR 09-015-023 from the National Aeronautics and Space Administration.

rotations. In addition, two solar days on Mercury are approximately equal in length to three synodic periods and to one terrestrial year, a coincidence largely responsible for the erroneous 88-day rotation period deduced from visual observations in the past (see Cruikshank and Chapman, 1967; Camichel and Dollfus, 1968). With the fundamental period of insolation equal to 176 days (1.52×10^7 sec) and a thermal conductivity similar to that of the Moon, the thermal skin depth on Mercury will be on the order of 10 cm, so that observations of the phase effect at microwave wavelengths that also arise at depths of tens of centimeters constitute a powerful tool for investigating thermal properties of the layers of the subsurface that experience a significant diurnal temperature variation. Following the suggestion of Johnson (1968), we shall call this part of the planetary subsurface the epilith.

Spectroscopic investigations by Bergstralh, Gray, and Smith (1967) and by Belton, Hunten, and McElroy (1967) have established that any atmosphere that Mercury may possess is too tenuous to have a significant effect on the temperature, a conclusion also reached on photometric grounds by Sagan (1966). In the absence of an atmosphere, the temperature in the epilith can be found as a function of time and depth by a solution of the one-dimensional heat-conduction equation, once the periodic variation of insolation and the thermal properties of the subsurface material are specified. Gary (1967) and Belton et al. (1967) have done this for a sinusoidal variation of the insolation during the daylight hours. Because of the high orbital eccentricity of Mercury, however, any point on the surface experiences an insolation that, while periodic with period 1.52×10^7 sec, is not sinusoidal and may differ markedly from the insolation at points at other planetary longitudes (see Soter and Ulrichs, 1967). The eccentricity enters in two ways. First, the variation in distance from the Sun produces a solar "constant" that varies by more than a factor of 2 from perihelion to aphelion. There thus exist longitudes on Mercury where the insolation is greater when the Sun is only 30° above the horizon than when it is overhead. Second, the changing orbital angular velocity causes the apparent speed of the Sun across the sky to vary; near perihelion the angular velocity of revolution actually slightly exceeds the angular

velocity of rotation, and the apparent planetocentric solar motion becomes retrograde. At some points on the planet, the Sun has two risings and two settings each solar day. The two effects of the eccentricity reinforce one another, with the largest flux coming at a time when the Sun is practically stationary and the smallest flux when the angular rate of the Sun across the sky is largest. The resulting variations in total heating are very great; the two longitudes (180° apart) that see the Sun overhead at perihelion receive more than twice the total energy per period than the longitudes 90° away receive, where the Sun is always small and rapidly moving while near the zenith.

Since the heat budget varies with planetocentric longitude, so will the temperature structure. These variations should be apparent in observed infrared and microwave temperatures. It is therefore insufficient to consider the observed temperatures as a function of only one celestial mechanical variable, the phase angle, as has been done for other planets (see, e. g., Pollack and Sagan, 1965). In this report, the microwave and infrared brightness temperatures are given as functions not only of local time on Mercury (as measured by the phase angle Φ) but also of the position of the sub-Earth point on the planet, as specified by the heliocentric longitude η. This choice of a second variable eliminates the ambiguity in the analysis of Mercury by Vetuchnovskaya and Kuzmin (1967), who use radius vector for the second variable.

In this report, I discuss the numerical computation of surface and subsurface temperatures and of the corresponding disk-averaged radio brightness temperatures for a range of physical models for the epilith. Thermal conductivities that incorporate a radiation term are included. The predictions of these models are then compared with the existing data. Of course, numerical models such as these are possible only for an idealized planet, and the results will not necessarily reproduce the behavior of the real planet. The plausibility of the basic assumptions can be estimated, but basically their justification must lie in the ability of the models to reproduce the observations. There is no assurance that a model that does reproduce the observations is a unique or necessarily a realistic description of the planet.

But within these restrictions, the construction of idealized models is a powerful tool for interpreting existing data and for indicating crucial observations that need to be made in the future, and the models described below do seem to offer valuable insights into the nature of the Mercurian subsurface.

2. COMPUTATIONAL TECHNIQUES

2.1 Thermometric Temperature Structure

In all the models I have computed, the subsurface material of Mercury (down to the depth of penetration of the diurnal thermal wave) is assumed to be horizontally and vertically homogeneous. Because the thickness of the layer involved in the diurnal temperature cycle is much less than the radius of the planet and also, it is assumed, much less than the radius of curvature of typical surface topography, the temperature structure is taken to be horizontally uniform, and all energy transport is along the normal to the surface. Since the surface itself is assumed spherical, the angle of incidence of solar radiation is a known function of the planetocentric coordinates of a surface point and of the orbital position of the planet.

Consider a subsurface material characterized by a density ρ (g cm^{-3}), a specific heat capacity c (cal g^{-1} deg^{-1}), and a thermal conductivity K(T) (cal sec^{-1} cm^{-2} deg^{-1}). With the assumption of plane-parallel geometry, the heat-conduction equation in the material is

$$\rho c \frac{\partial T}{\partial t} = \frac{\partial}{\partial x}\left[K(T) \frac{\partial T}{\partial x} \right] \quad . \tag{1}$$

We neglect any possible sources or sinks of thermal energy in the subsurface (cf. Walker, 1961). We shall consider only a slab of depth X, where X is large enough that the time variation of T(X) is negligible. The boundary condition at X is

$$K(T) \left(\frac{\partial T}{\partial x} \right)_{x=X} = F_0 \quad , \tag{2}$$

where the flux F_0 may be due to energy conducted upward from hotter regions below. At the surface, the boundary condition is

$$K(T)\left(\frac{\partial T}{\partial x}\right)_{x=0} = E(T)\,\sigma\,T^4(0) - (1 - A)\,I(t) \quad , \tag{3}$$

where σ is the Stefan-Boltzmann constant (1.35×10^{-12} cal cm^{-2} deg^{-4} sec^{-1}), A is the bolometric albedo, and I(t) is the time-variable insolation. The integrated radiometric emissivity E(T) is found from the monochromatic emissivity by the relation

$$E(T) \equiv \frac{1}{\sigma\,T^4} \int_0^\infty E_\nu B_\nu(T)\, d\nu \quad , \tag{4}$$

where $B_\nu(T)$ is the Planck function.

The homogeneous, plane-parallel heat-conduction equation with these boundary conditions was solved analytically 20 years ago under the simplifying restrictions of temperature-independent conductivity and daytime dependence of insolation on time that was sinusoidal (Wesselink, 1948; Piddington and Minnett, 1949; Jaeger, 1953). More recently, Muncey (1958, 1963) has obtained a solution for the case in which conductivity is linearly dependent on temperature. However, it is most profitable to obtain numerical solutions to the heat-conduction equation by use of a digital computer, and it is this approach that has been applied recently to the Moon (see, e. g., Linsky, 1966). The numerical approach permits solutions involving complex variations of thermal properties with temperature and depth, so that the choice of models is not limited by the thermal parameters that can be incorporated.

The dependence of the thermal conductivity on temperature is not well known for materials that might be expected to make up the subsurface of Mercury. The primary temperature effect is, however, known to be an increase of conductivity at higher temperatures due to the transport of energy by radiation as well as by ordinary contact conduction. When energy transport

in the Earth and Moon has been dealt with, conductivities have been considered that vary as the first, second, or third power of the temperature (see, e. g., MacDonald, 1963; Linsky, 1966; Troitsky, 1967; Troitsky, Burov, and Alyoshina, 1968). To represent the range of temperature dependence that may apply, I have considered the following two forms:

1) Temperature independence: $K = K_0$

2) Temperature-cubed dependence: $K(T) = K_0 + BT^3$.

For these two cases, the heat-conduction equation becomes

$$\rho c \frac{\partial T}{\partial t} = K_0 \frac{\partial^2 T}{\partial x^2} \tag{5}$$

$$\rho c \frac{\partial T}{\partial t} = (K_0 + BT^3) \frac{\partial^2 T}{\partial x^2} + 3BT^2 \left(\frac{\partial T}{\partial x}\right)^2 \quad . \tag{6}$$

Since equation (6) reduces to equation (5) in the case that $B = 0$, the temperature-independent models are considered in the following to be a special case of the temperature-cubed dependence of conductivity.

Equation (6) can be solved numerically when written in finite difference form. Let us consider a time increment Δt and a depth increment Δx, with $T_m^n = T(x = m\,\Delta x,\ t = n\,\Delta t)$. Then, with the use of central and forward differences, equation (6) becomes

$$T_m^{n+1} = T_m^n + C \left\{ \left[K_0 + B(T_m^n)^3 \right] \left[T_{m+1}^n - 2T_m^n + T_{m-1}^n \right] + \left[\frac{3}{4} B(T_m^n)^2 \right] \left[(T_{m+1}^n)^2 - 2T_{m+1}^n T_{m-1}^n + (T_{m-1}^n)^2 \right] \right\} \quad , \tag{7}$$

where

$$C \equiv \frac{\Delta t}{\rho c (\Delta x)^2} \quad .$$

In order to ensure stability of the numerical solution against perturbations, the coefficient $K \cdot C$ must be less than 1/2 (Munro, 1964). The temperature at the surface, T_0^n, is found when the upper boundary condition (3) is written as

$$K_0\left[\frac{-T_2^n + 4T_1^n - 3T_0^n}{2(\Delta x)}\right] + B\left(\frac{T_1^n + T_0^n}{2}\right)^3\left(\frac{T_1^n - T_0^n}{\Delta x}\right)$$

$$= E(T_0^n)\sigma(T_0^n)^4 - (1 - A)\,I(t) \quad . \tag{8}$$

This equation is solved numerically by Newton's method. As shown by Walker (1961), any fluxes that might originate from internal heat sources are negligible in comparison with the diurnal fluxes produced by the varying insolation. Therefore, a lower boundary condition of zero flux is assumed. The temperature of the bottom layer considered in the calculations is adjusted to give a zero net flux (averaged over one diurnal cycle) at all levels in the subsurface, and the accuracy with which this condition is fulfilled throughout the subsurface is a measure of the convergence of the numerical solution to a steady state.

For the temperature-independent case ($B = 0$), the diurnal period is divided into 176 time intervals of 8.6×10^4 sec. The depth increment Δx is then calculated directly from the requirement that $K \cdot C = 0.4$, and the maximum depth considered is $X = 30 \cdot \Delta x$. Where $B > 0$, the depth scale is calculated as above by use of $K(T)$ evaluated at $T = 350°K$. To ensure stability over the entire temperature range, the time increment is then decreased so that $K \cdot C$ is less than 0.4 for a temperature of 710°K, which is the highest value ever reached on Mercury. With these values for Δx and Δt established, the computations are continued through five or more diurnal cycles, the temperature being adjusted at depth X at the end of each cycle as needed, until the temperatures at each depth throughout the cycle converge to their steady-state values.

The insolation I(t) is a function of both planetocentric and orbital coordinates. The orbital position is specified by the heliocentric longitude η; the planetocentric coordinates are longitude and latitude. In all the computations presented here, the obliquity of the axis of rotation of Mercury is taken to be zero, a result consistent with, but not demonstrated by, the radar data (Dyce et al., 1967). If we treat the Sun as a point source and define LHA(t, ℓ) as the local hour angle (LHA) of the Sun at latitude ℓ, the insolation is given by

$$I(t, \ell, \phi) = \frac{I_0}{[r(t)]^2} \cos(\phi) \cos[\mathrm{LHA}(t, \ell)] \quad \text{for} \quad \cos(\mathrm{LHA}) \geq 0,$$

$$= 0 \quad \text{for} \quad \cos(\mathrm{LHA}) < 0 \quad , \tag{9}$$

where I_0 is the solar constant (1.388×10^6 erg cm^{-2} sec^{-1}) and r(t) is the radius vector in astronomical units. The local hour angle is found from the axial rotation rate $\Omega = (6\pi/1.52 \times 10^7)$, the orbital angular position η, and the longitude

$$\mathrm{LHA}(t, \ell) = (t - t_0)\Omega - [\eta(t) - \eta(t_0)] + \ell \quad . \tag{10}$$

The quantities r(t) and $\eta(t)$ are tabulated in the American Ephemeris and Nautical Almanac.

I have used the CDC 6400 computer of the Smithsonian Astrophysical Observatory (SAO) to find the thermometric temperature in the subsurface as a function of η for particular points (ϕ, ℓ) on the surface of Mercury, using a variety of assumed thermal and photometric parameters. In the case of temperature-independent conductivity, I have checked my results for the surface temperatures against those found by Soter and Ulrichs (1967), who used a finer grid of time and depth increments and also allowed for the finite angular size of the Sun. The agreement is excellent, verifying the adequacy of my more economical computing procedures.

2.2 Radio Brightness Temperatures

Since thermometric temperatures have not been measured on Mercury, it is necessary to use the temperatures described above to compute radio brightness temperatures at microwave wavelengths to be compared with existing data. From a temperature distribution T(x), we wish to find $T_R(\lambda, \theta)$, the radio temperature at wavelength λ as seen at an angle θ from the normal to the surface.

The angle θ is the direction of the ray in vacuo. The ray direction θ' in the subsurface is given by Snell's Law:

$$\sin \theta' = \frac{\sin \theta}{n(\lambda)} \quad ,$$

where $n(\lambda)$ is the index of refraction for the radio wave in the subsurface. Using the Rayleigh-Jeans approximation, we have the equation of radiative transfer in a solid:

$$T_R(\lambda, \theta) = [1 - R(\lambda)] \int_0^\infty T(x) \exp\left[\frac{-k(\lambda)x}{\mu}\right] \left(\frac{k(\lambda)}{\mu}\right) dx \quad , \tag{11}$$

where $k(\lambda)$ is the absorption cross section per unit volume (cm^{-1}), $R(\lambda)$ is the surface reflectivity, and $\mu \equiv \cos \theta'$. In order to evaluate the integral (11) from a finite set of computed temperatures T_m, we sum the contributions from each layer, assuming a linear temperature gradient within the layer. For the layer extending from x_{m-1} to x_m, integration of equation (11) by parts illustrates the dependence on the temperature gradient:

$$T_R(m) = (1 - R)\left\{T_{m-1} \exp\left(\frac{-kx_{m-1}}{\mu}\right) - T_m \exp\left(\frac{-kx_m}{\mu}\right) + \left(\frac{\mu}{k}\right)\left(\frac{dT}{dx}\right)\left[\exp\left(\frac{-kx_{m-1}}{\mu}\right) - \exp\left(\frac{-kx_m}{\mu}\right)\right]\right\} . \tag{12}$$

If $m = 2$ and $x_1 = 0$, and we let x_2 approach infinity, equation (12) reduces to the familiar second Eddington-Barbier relation.

To obtain the total brightness temperature T_R, the individual contributions of equation (12) are summed over M layers. Below the Mth level, the temperature is taken to be constant at T_M. Then T_R is given by

$$T_R = (1 - R)\left\{T_1 + \left(\frac{\mu}{k}\right) \sum_{m=1}^{M} \left(\frac{T_m - T_{m-1}}{x_m - x_{m-1}}\right) \left[\exp\left(\frac{-kx_{m-1}}{\mu}\right) - \exp\left(\frac{-kx_m}{\mu}\right)\right]\right\} . \quad (13)$$

This equation is used to compute the individual radio temperatures that must then be combined to reproduce the average brightness temperature of the unresolved planetary disk.

2.3 Disk-Averaged Temperatures

In determining the way to combine individually computed brightness temperatures to give disk-averaged temperatures, I neglected the inclination of Mercury's orbit to the ecliptic. Thus, the subterrestrial and the subsolar points are always taken to lie on the equator of Mercury. Since the orbital inclination is only 7°, errors introduced by this simplification are less than order $(1 - \cos^{1/4} 7°) \cong 0.1\%$ and so are not significant.

For convenience in visualizing the geometry of the situation, we may consider Mercury fixed at a value of η and examine its appearance from a moving Earth. The phase angle Φ is the planetocentric angle between Sun and Earth. It is clear that the subterrestrial longitude on Mercury has a local hour angle of the Sun equal to Φ. Further, we know the relationship at any time among η, LHA, and ℓ [equation (10)]. We can readily eliminate the variables LHA and ℓ and express the temperatures in terms of the celestial mechanical variables (η, Φ), which are the most convenient variables to associate with the observations.

In constructing thermal models of Mercury, I have computed temperatures as a function of time for the grid of planetary coordinates spaced 30° apart in latitude and longitude. From the T(x) found at each of these points at a given time, three radio brightness temperatures are computed, corresponding to angles of view of 0°, 30°, and 60° from the local normal. These directions all lie in a plane parallel to the ecliptic. The temperatures at each longitude are averaged over latitude, the points at latitudes 0°, 30°, and 60° being weighted in the ratio of the projected areas of the strips of which they are the centers (0.329:0.556:0.115). The numerical computation of disk-averaged temperatures is then reduced to finding the weighted average of the temperatures at the subterrestrial longitude ℓ_0 at normal incidence, at the longitudes $\ell_0 \pm 30°$ at a 30° angle of incidence, and at longitudes $\ell_0 \pm 60°$ at a 60° angle of incidence, all of which are already computed. The appropriate weights are (0.096:0.266:0.276:0.266:0.096).

The computational procedure described above requires that a complete temperature structure be computed for 18 individual points on the surface of the planet. It is clear, however, that the three points computed at each longitude will have exactly the same insolation cycle, except for the $\cos\phi$ term in equation (9). It therefore seems worthwhile to look for an intermediate latitude where the temperature will always be equal to the weighted mean of the temperatures at latitudes 0°, 30°, and 60°. If this latitude does not vary with wavelength of observation or with the assumed parameters of the model, its use will cut total computation time by more than a factor of 2.

The total energy incident on the surface is proportional to $\cos\phi$. If we assume that all the temperatures scale as $(\cos\phi)^{1/4}$, the latitude ϕ_0, where the temperature is equal to the latitude-averaged mean of all the temperatures, is given by

$$(\cos\phi_0)^{1/4} = \frac{\int_{\text{disk}} (\cos\phi)^{1/4} \cos\phi \cos\ell \, d\omega}{\int_{\text{disk}} \cos\phi \cos\ell \, d\omega} \qquad (14)$$

When the solid angle $d\omega$ is written in terms of $d\phi$ and $d\ell$, equation (14) reduces to

$$(\cos \phi_0)^{1/4} = \frac{\int_0^{\pi/2} (\cos \phi)^{9/4} \, d\phi}{\int_0^{\pi/2} (\cos \phi)^2 \, d\phi} \quad . \tag{15}$$

Evaluation of equation (15) gives $\phi_0 = 33°$.

From an examination of the computed temperatures for a wide variety of models and wavelengths, I concluded that temperatures found for $\phi_0 = 30° \pm 2°$ agree within 0.5% at all times with the latitude-averaged temperatures. An examination of equation (14) indicates that if $\phi_0 = 30°$ rather than 33°, the power-law dependence of the temperature is slightly stronger than $(\cos \phi)^{1/4}$; in other words, it appears that the temperatures at higher latitudes are somewhat hotter than would be expected from the idealized $(\cos \phi)^{1/4}$ law. In any case, the actual brightness temperatures computed for $\phi_0 = 30°$ and 33° differ by less than 1%, so that it matters very little which is used. In computing a grid of models, I have substituted the temperatures calculated at $\phi_0 = 30°$ for those obtained by actual averaging over latitude.

2.4 Infrared Brightness Temperatures

Brightness temperatures have been measured for Mercury in the 8- to 14-μ infrared window as well as at microwave frequencies, and I have computed infrared temperatures from the models to compare with these data. Since the opacity of the surface materials of Mercury is almost certainly very great at micron wavelengths, I have taken the effective emitting region in the infrared to be the actual surface. The brightness temperature is then computed from the surface thermometric temperature by multiplying by the fourth root of the emissivity, although for greater accuracy, the nth root, where $n = 1.439/\lambda T$, should be used at temperatures below 300°K for this

spectral band (see Morrison, 1968b). Since only center-of-disk temperatures are given, possible dependence of emissivity on direction (see Sinton, 1962) does not introduce any additional error.

2.5 The Computer Program

I have written a FORTRAN IV computer program to execute all the computational steps described above. In Figure 1, an outline flow diagram of this program is given.

MERCURY, the main control program, begins the calculation of each model by reading the values of the parameters $(K\rho c)_{350}^{-1/2}$ and R_{350} defined at 350°K. Here, R_{350} is the ratio $B \cdot (350)^3/K_0$, where K_0 is the temperature-independent contribution to the conductivity. Because longitudes separated by 180° on the planet undergo identical thermal cycles, it is necessary to compute temperatures only for ℓ = 0°, 30°, 60°, 90°, 120°, and 150°. The diurnal cycle is two orbital periods in duration, so that two temperatures at each of these longitudes are associated with each η. The second of these temperatures is assigned by the program to longitude $\ell + 180°$, so that the resulting temperatures are unique functions of η and ℓ, with ℓ running from 0° to 330°.

Subroutines ORBIT, CONDUCT, and PHOTON compute the thermometric temperatures T(x) at each value of η and ℓ. ORBIT generates the insolation given by equation (9). CONDUCT finds T(x) on the assumption of temperature-independent conductivity [K = K(T = 350°)] ; PHOTON then takes this solution as a starting point for the determination of T(x) by equations (7) and (8). Subroutine RADTEMP converts the thermometric temperatures to radio brightness temperatures at seven wavelengths: λ = 1.2 mm, 3.4 mm, 8.0 mm, 1.9 cm, 3.75 cm, 11.3 cm, and 21.0 cm; it also finds the equatorial infrared brightness temperature. Function subroutine RADIO computes T_R for each value of λ and θ, using equation (10). These temperatures are

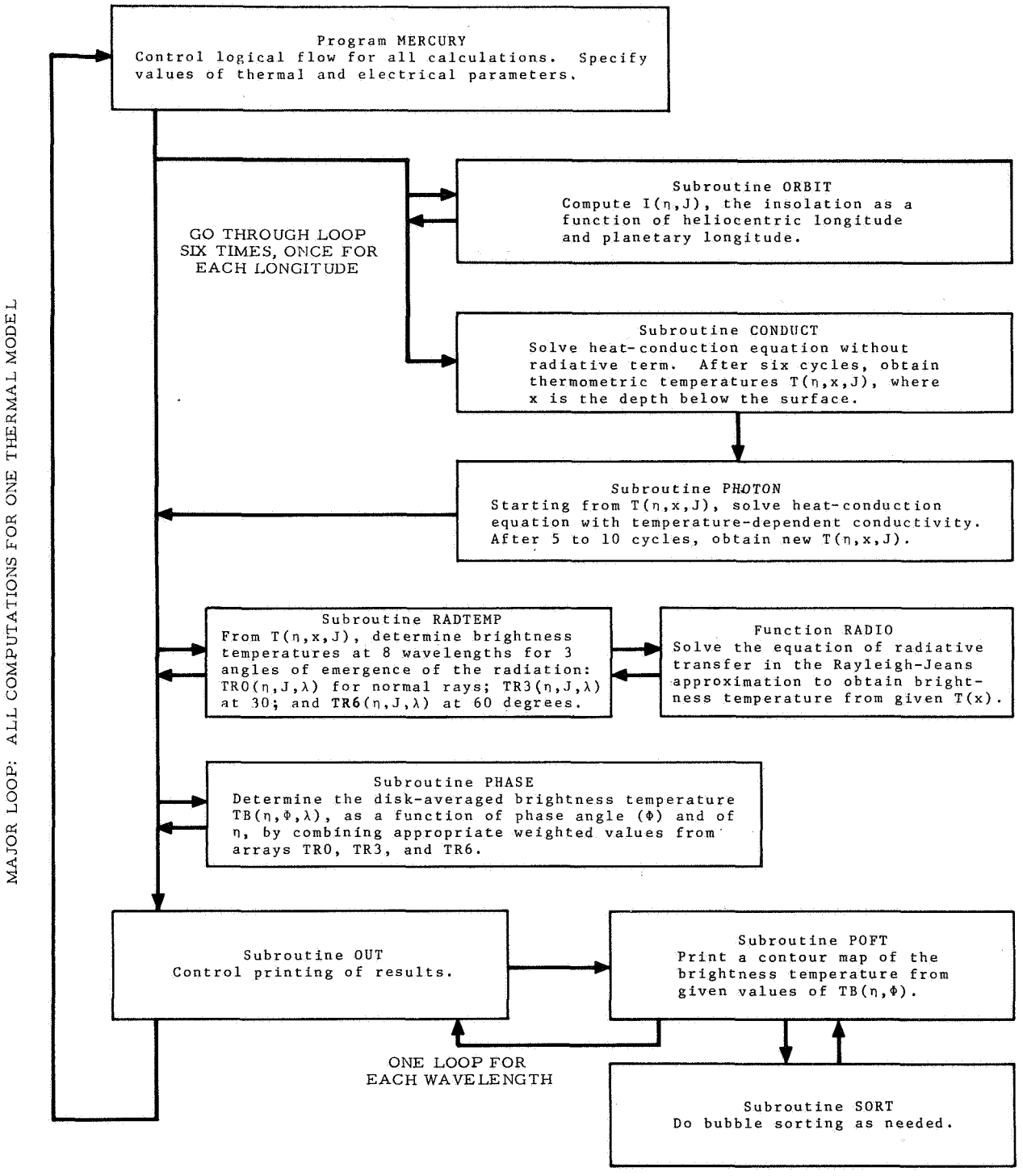

Figure 1. Flow diagram of the main program and subroutines used to calculate Mercury models.

combined by subroutine PHASE to give disk-averaged temperatures expressed as a function of (η, Φ). Using subroutines OUT, POFT, and SORT, the program presents the results of these calculations in the form of contour maps giving the brightness temperature in the (η, Φ) plane. For each model, eight maps are generated, one for each of the wavelengths considered.

This computer program was written for SAO's CDC 6400 computer. On this machine, with the use of the SCOPE 3.0 compiler, the central processor computation times for a typical model have been determined to be the following:

CONDUCT	15 sec
PHOTON	80
RADTEMP and PHASE	10
All others	15
Total time	120 sec

This total time is for a single latitude; if the computations are carried out for three latitudes, the total time is increased to about 315 sec per model.

2.6 Computational Errors

Numerical computation of models of Mercury using finite-difference techniques necessarily introduces some random errors into the resulting brightness temperatures. In a number of test cases, I have estimated the magnitude of the uncertainty in the numerical results.

The errors in the insolation introduced by subroutine ORBIT are negligible. Thermometric temperatures found by subroutine CONDUCT have errors of less than 1%, but these increase when temperature-dependent conductivities are considered by PHOTON. The largest uncertainties are associated with the upper boundary in CONDUCT and with the lower boundary in PHOTON; in the latter case, the errors may reach 2%. It does not seem worthwhile, however, to use the extra machine time required to reduce these errors below the values quoted.

Radio brightness temperatures are computed very accurately when the effective depth of emission (k/μ) is several times the depth increment Δx, as can be seen from equation (12). However, the millimeter radiation arises primarily in the upper one or two layers for most models, and here the assumption of a linear gradient within each layer introduces some problems. These errors are still probably less than 2% in the brightness temperature.

A typical error introduced by the use of temperatures computed at $\phi_0 = 30°$ as a substitute for direct averaging over latitude is less than 0.5%. Averaging over longitude with use of a 30° grid will introduce errors of up to 1%. Of course, the center-of-disk infrared temperatures are as accurate as the surface thermometric temperatures, since no averaging is involved.

In the final presentation of the numerical results as contour plots, a certain amount of smoothing takes place, which tends to reduce the effects of small random errors in the temperatures. I conclude that the errors in the plotted brightness temperatures are generally less than 2% for the centimeter wavelengths but may be as high as 5% at the shortest radio wavelength, $\lambda = 1.2$ mm.

3. SPECIFICATION OF NUMERICAL PARAMETERS

The computer program outlined in the preceding section requires that numerical values be given for a number of physical properties of the epilith of Mercury. To avoid the necessity for a many-dimensional grid of models, I have adopted standard values for most of these parameters and have computed models with only the contact thermal conductivity and the radiative conductivity allowed to vary.

3.1 Photometric Properties

From a review of the observational data, de Vaucouleurs (1964) finds a visual Bond albedo of 0.058 and notes (see also Sagan, 1966) that the variation of albedo with wavelength is very similar for Mercury and for the Moon. Since the ultraviolet and infrared phase curves are unknown, de Vaucouleurs is unable to specify a value for the bolometric albedo. In their thermal calculations, Soter and Ulrichs (1967) adopt a bolometric albedo equal to the visual albedo of 0.058, while Belton et al. (1967) use the value of 0.23 by analogy with the high lunar albedo employed by Jaeger (1953). Linsky (1966), using the data given by Harris (1961), finds a bolometric albedo for the Moon of 0.12. For these calculations, I have adopted an albedo of 0.10, similar to that of the Moon and consistent with the existing measurements for Mercury. The temperatures scale with the albedo as $(1 - A)^{1/4}$, so the change in temperature is only 1% for an albedo differing by ± 0.05 from the adopted value.

Total-reflectance measurements of a number of terrestrial igneous rocks in a wide range of particle sizes have been made in the wavelength range 0.5 to 22 μ by Hovis and Callahan (1966). To the degree that these substances may be considered representative of the surface of Mercury, these data can be used to determine the radiometric emissivity. Photometric and polarimetric evidence indicates that the bulk of the surface material on Mercury is granular or dusty; this fact simplifies the computation of emissivity, since

the data of Hovis and Callahan indicate that the peculiar spectral features of rocks of different composition show most strongly in solid samples and become much less prominent in pulverized samples. Therefore, I have chosen to consider only two of their spectral reflectance curves, both for mixed samples of pulverized rock: one of size 1 to 2 mm and one of less than 0. 038 mm. The most prominent feature in the spectra of these samples is the broad absorption by water of crystallization or water of constitution near 3 μ. Sinton (1967) has observed this band in reflection spectra of Mars, where its depth is comparable to that observed in these terrestrial samples. Whether it exists on other planets is not known, but its absence would change the values of the radiometric emissivity only for temperatures above 600° K. Applying equation (4) to these data, I have obtained the emissivities illustrated as a function of temperature in Figure 2. The monochromatic emissivities were assumed constant beyond 22-μ wavelength. For the models presented in this report, I have used the constant radiometric emissivity of 0. 94 indicated in Figure 2 as being appropriate for small particle sizes.

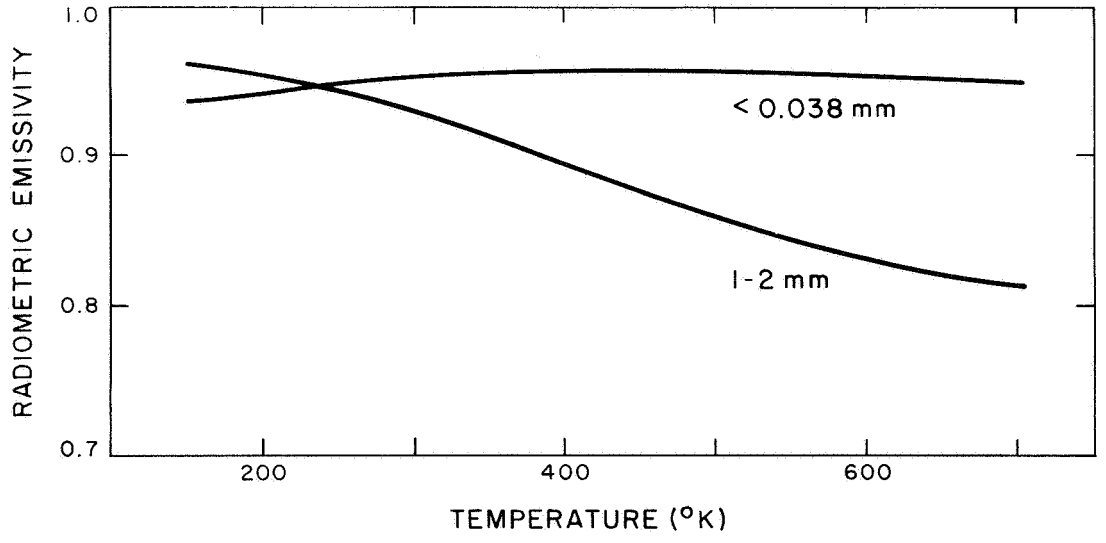

Figure 2. Radiometric emissivities of pulverized terrestrial rocks, computed from the reflectance measurements of Hovis and Callahan (1966). Two distributions of particle sizes are shown.

A similar calculation of the average emissivity in the 8- to 14-μ atmospheric window gives a value of 0.94, practically independent of either temperature or particle size, and this is the value used to convert thermometric surface temperatures to infrared brightness temperatures. These brightness temperatures are primarily sensitive only to changes in the ratio of these two emissivities, not simply to the 8- to 14-μ emissivity.

3.2 Bulk Properties

The density ρ (g cm^{-3}) and the specific-heat capacity c (cal g^{-1} deg^{-1}) enter the calculations primarily through the thermal parameter $(K\rho c)^{-1/2}$. The subsurface density on Mercury can be expected to fall between 3.0, a value typical for solid terrestrial rock, and the value of 0.6 to 1.2 recently found for the uppermost layer on a lunar mare (Christensen, Batterson, Benson, Chaote, Jaffe, Jones, Ko, Spencer, Sperling, and Sutton, 1968; Campbell, Ulrichs, and Gold, 1968). On the Moon, the density increases with depth from these low values to a limiting value of about 2.8 tens of centimeters below the surface, and a density of 1.5 g cm^{-3} is considered characteristic of the upper 10 cm of the epilith (Jaffe, Batterson, Brown, Christensen, Gault, Lucas, Norton, Scott, Shoemaker, Sutton, and Turkevich, 1968; Scott and Roberson, 1968). For Mercury, I assume a constant density of 1.5 g cm^{-3}. Almost all abundant minerals have specific-heat capacities near 0.20 cal g^{-1} deg^{-1} (International Critical Tables, 1933), so this value is adopted for Mercury. The product ρc is then 0.30 cal cm^{-3} deg^{-1}.

3.3 Electrical Properties

The only experimental measurements of the electrical properties of Mercury are the radar cross sections of about 6% observed at wavelengths from 12.5 to 68 cm (see Pettengill, Dyce, and Campbell, 1967). For a smooth surface, the corresponding value of the relative dielectric constant ϵ is 2.7; if we employ a directivity factor g = 1.1 as suggested for the Moon (Pettengill, 1965), then ϵ = 2.9. These dielectric constants are similar to

that of the Moon but are somewhat smaller than those of Venus, Mars, and terrestrial rocks. Loose, dry sand, however, does have a dielectric constant of about 3 (Pettengill, 1965). Assuming the surface of Mercury behaves as a pure dielectric with dielectric constant $\epsilon = 2.9$ at the wavelengths of interest, I have set the reflectivity R of equation (10) equal to 0.060 and the index of refraction equal to 1.7 for all radio wavelengths.

To calculate microwave temperatures from thermometric temperatures, we must also specify the absorption cross section per unit volume k (cm^{-1}). For most geochemically abundant materials, k can be expressed as k_0/λ, where k_0 is a constant that depends on the composition and porosity of the material. Pollack and Sagan (1965) have discussed the dependence of opacity on composition for a wide range of minerals and have found variations of more than 2 orders of magnitude. The value of k_0 of 0.10 found from microwave studies of the Moon (Weaver, 1965) is typical of loose, dry mineral samples and is the value adopted for Mercury. To a good first approximation, a given phase effect can be matched by models employing a range of thermal properties, so long as we also allow k_0 to vary in such a way that the ratio of electrical and thermal skin depths (see Section 3.4 below) is constant. This ambiguity does not exist for infrared observations, for which the radiation is assumed to originate at zero depth, but it does limit our ability to determine uniquely the thermal properties of Mercury from microwave observations alone.

3.4 Thermal Properties

With all the preceding parameters specified, the independent variables that specify the models are only the temperature-independent thermal conductivity K_0 (cal cm^{-1} sec^{-1} deg^{-1}) and the coefficient B of the temperature-dependent conductivity [see equation (6)]. For convenience, the independent variables actually used in the computation of thermal models were $\gamma_{350} = (K\rho c)^{-1/2}$ (cal^{-1} cm^2 $sec^{1/2}$ deg) and $R_{350} = B \cdot T^3/K_0$, both evaluated at T = 350°K.

For comparison with microwave temperatures, the models with no radiative term in the conductivity are more conveniently characterized by a parameter that does not depend for interpretation on the choice of microwave opacity. The thermal skin depth L_t is the depth at which the amplitude of the first harmonic in a Fourier analysis of the temperature is reduced to 1/e of its surface value, and the electrical skin depth L_e is the distance in which the energy of an incident electromagnetic wave is damped to 1/e of its incident value. The ratio of these depths is the dimensionless parameter δ, given by

$$\delta = \frac{L_e}{L_t} = 4.56 \times 10^{-4} \left(\frac{\lambda \rho c}{k_0}\right) \gamma \quad . \tag{16}$$

The parameter that we may wish to use instead of γ is then δ/λ (cm^{-1}); with our choice of numerical values, this is

$$\delta/\lambda = 1.37 \times 10^{-3} \gamma \ cm^{-1} \quad . \tag{17}$$

In the following sections, the variations of microwave temperature will be presented as a function of δ/λ.

Following Linsky (1966), we can interpret the value of the radiation coefficient B in terms of the mean spacing s between opaque radiating particles in the subsurface:

$$B = 4 E \sigma s \quad , \tag{18}$$

where E is the infrared emissivity, and σ is the Stefan-Boltzmann constant. A similar expression can be derived from the equations of radiative transfer in a continuous gray medium of opacity κ; if we consider an elementary volume several infrared optical depths below the surface, where the radiation field is nearly isotropic, we obtain

$$B = \frac{16}{3} \frac{\sigma}{\kappa \rho} \quad . \tag{19}$$

Except for the factor 3E/4, this result is identical to the preceding when the length s is identified with the photon mean free path $(\kappa\rho)^{-1}$. Thus, a determination of γ_{350} and R_{350} can lead to values for the thermal conductivity and the thermal photon mean free path in the subsurface of Mercury.

4. RESULTS OF CALCULATIONS

4.1 Contour Plots of $T_B(\Phi,\eta)$

As described in the preceding sections, each model is defined by specifying values for parameters γ_{350} and R_{350}; contour plots of brightness temperature as a function of phase angle and heliocentric longitude are then generated. A comparison of preliminary models with the observations at 1.9 cm (Morrison and Sagan, 1967) and at 3.4 mm (Morrison, 1968a) indicates that approximate fits to the data are obtained with $\gamma_{350} \simeq 500$ cal^{-1} cm^2 sec$^{1/2}$ deg and $R_{350} \simeq 0$. I have therefore chosen for presentation those models with $\gamma_{350} = 250$, 500, and 1000 cal^{-1} cm^2 sec$^{1/2}$ deg. In Figures 3 through 8, contour plots are given for $R_{350} = 0.0$ at wavelengths of 0.12, 0.34, 0.80, 1.90, 3.75, and 11.30 cm. Figure 9 gives a similar plot of the center-of-disk infrared brightness temperature. Models with $R_{350} \neq 0$ will be presented in a later section. Phase curves for wavelengths intermediate between those given can easily be found from the plots by linear interpolation between phase curves obtained for the bracketing wavelengths.

It is apparent from these figures that for a given electrical skin depth, and hence for a given physical depth, the amplitude of the temperature variation increases with decreasing thermal parameter γ_{350}. It is for this reason that, in this report, the commonly employed term "thermal inertia" is not used for the reciprocal of the thermal parameter. This term was introduced when only the amplitude of the surface temperature variation was considered, where a large "inertia" implies a damped temperature cycle. But in the subsurface, increasing this inertia actually increases the temperature variation, so that the term thermal inertia is confusing. This term is therefore better not used.

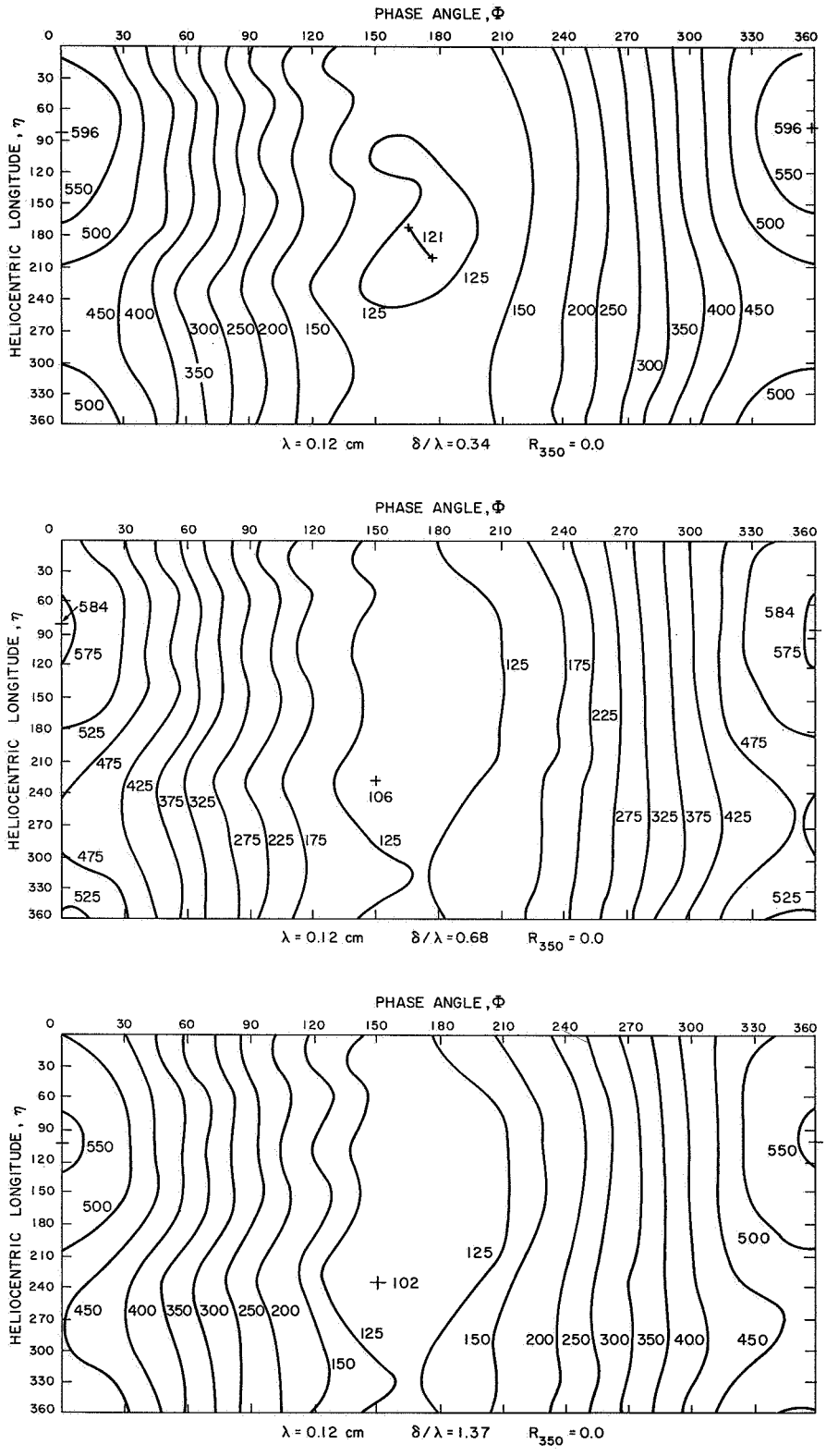

Figure 3. Computed brightness temperature as a function of Φ, η, and γ_{350} for $R_{350} = 0$ and $\lambda = 1.2$ mm.

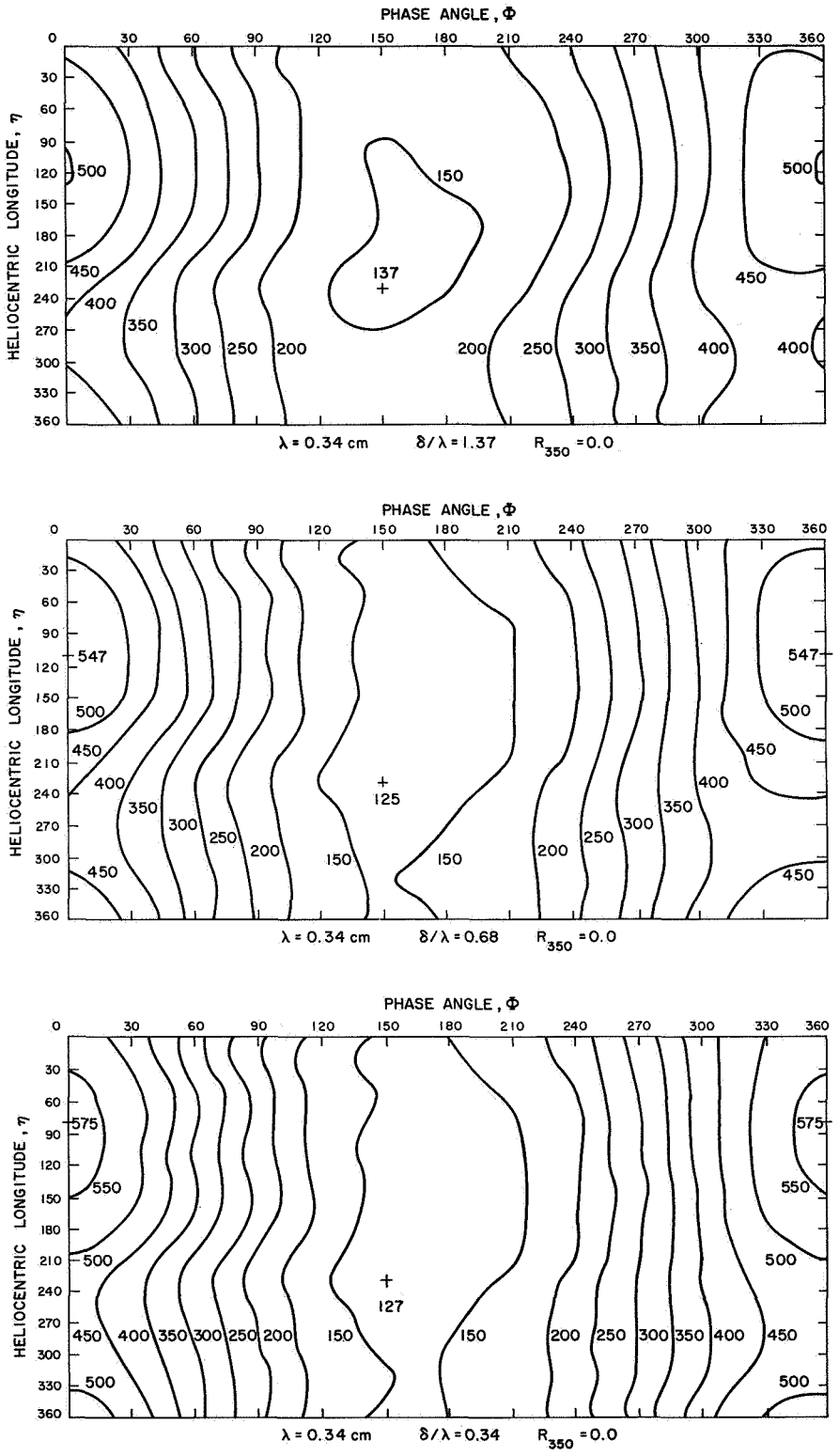

Figure 4. Computed brightness temperature as a function of Φ, η, and γ_{350} for $R_{350} = 0$ and $\lambda = 3.4$ mm.

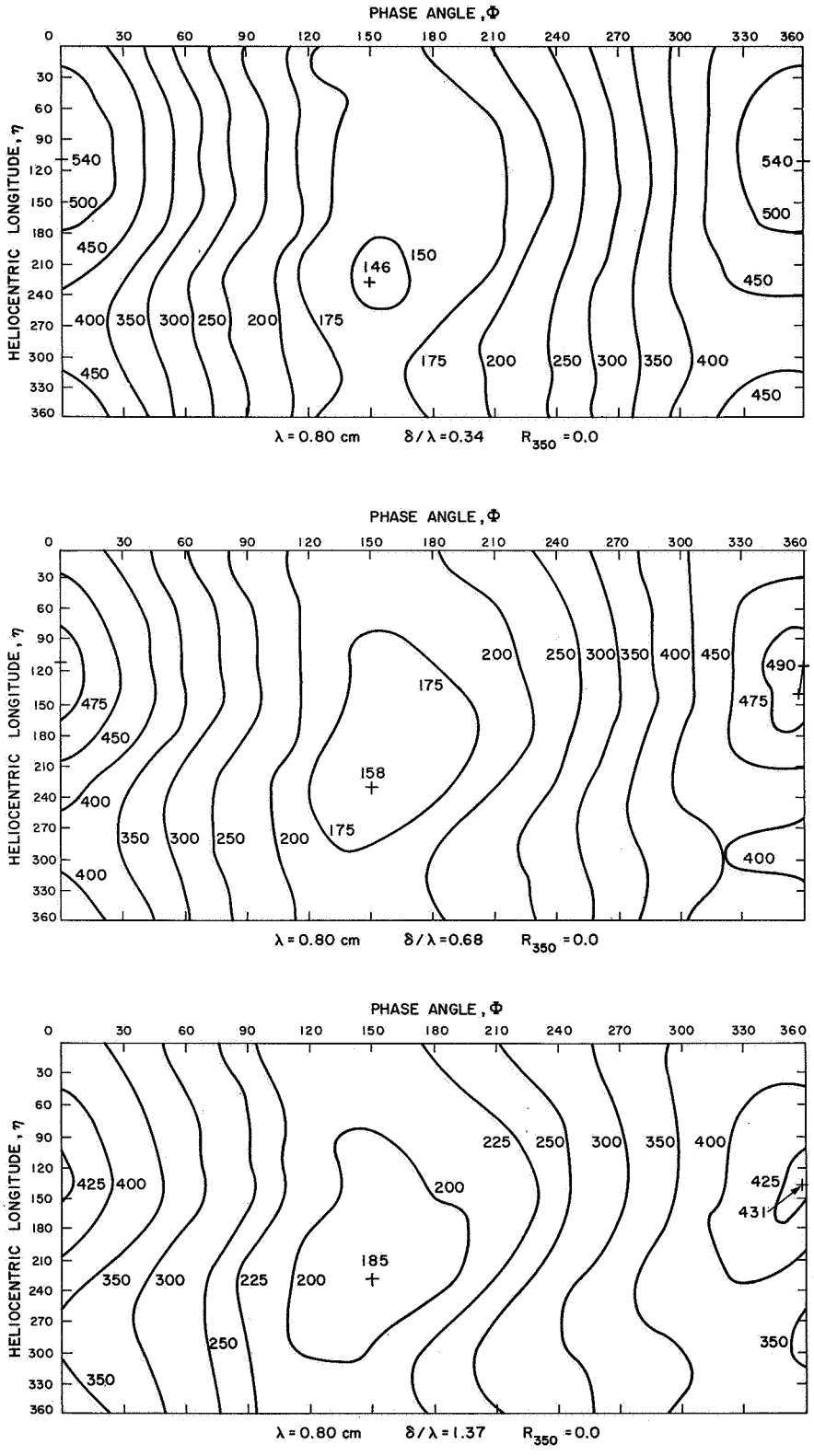

Figure 5. Computed brightness temperature as a function of Φ, η, and γ_{350} for $R_{350} = 0$ and $\lambda = 8.0$ mm.

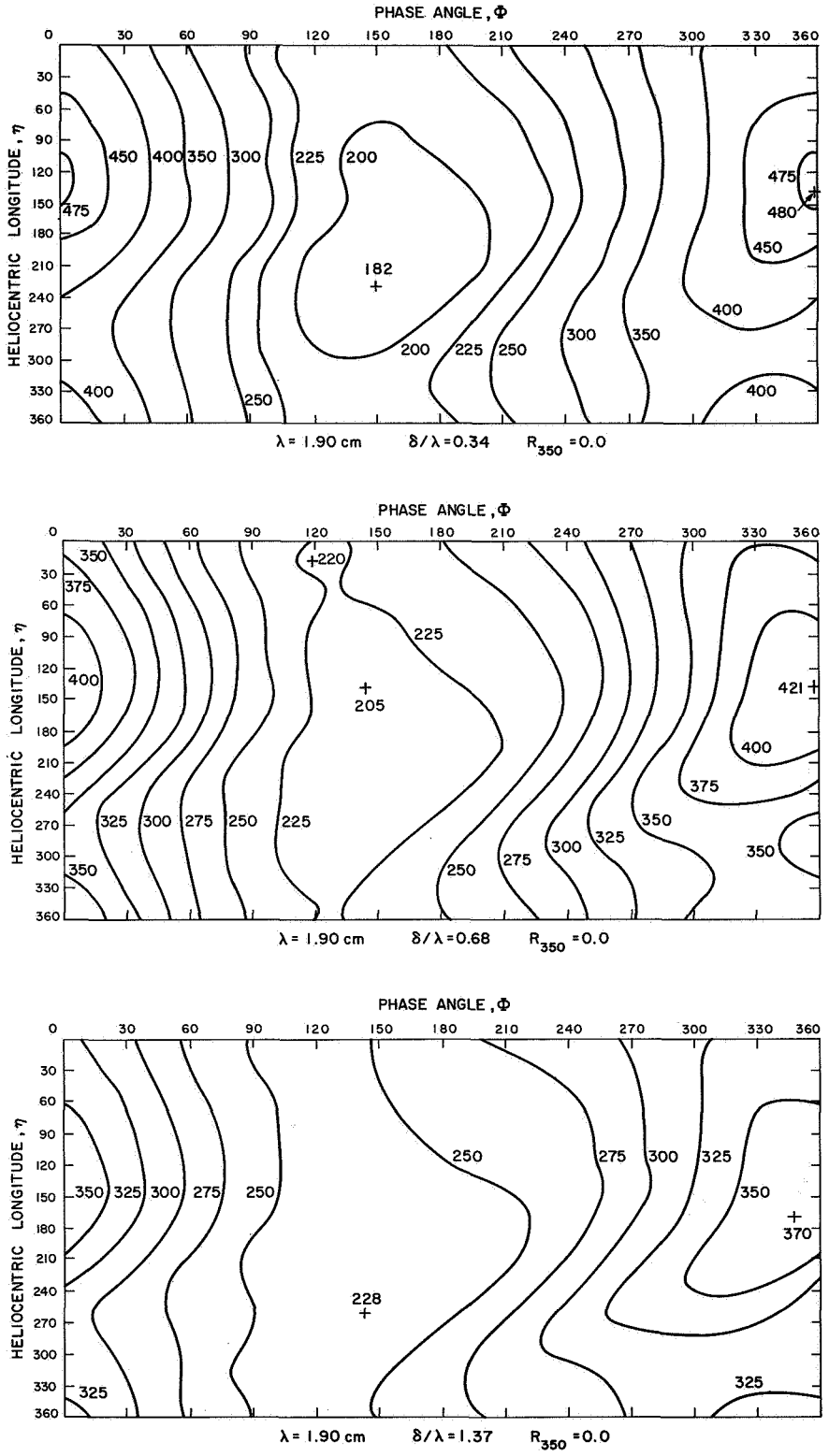

Figure 6. Computed brightness temperature as a function of Φ, η, and γ_{350} for $R_{350} = 0$ and $\lambda = 1.90$ cm.

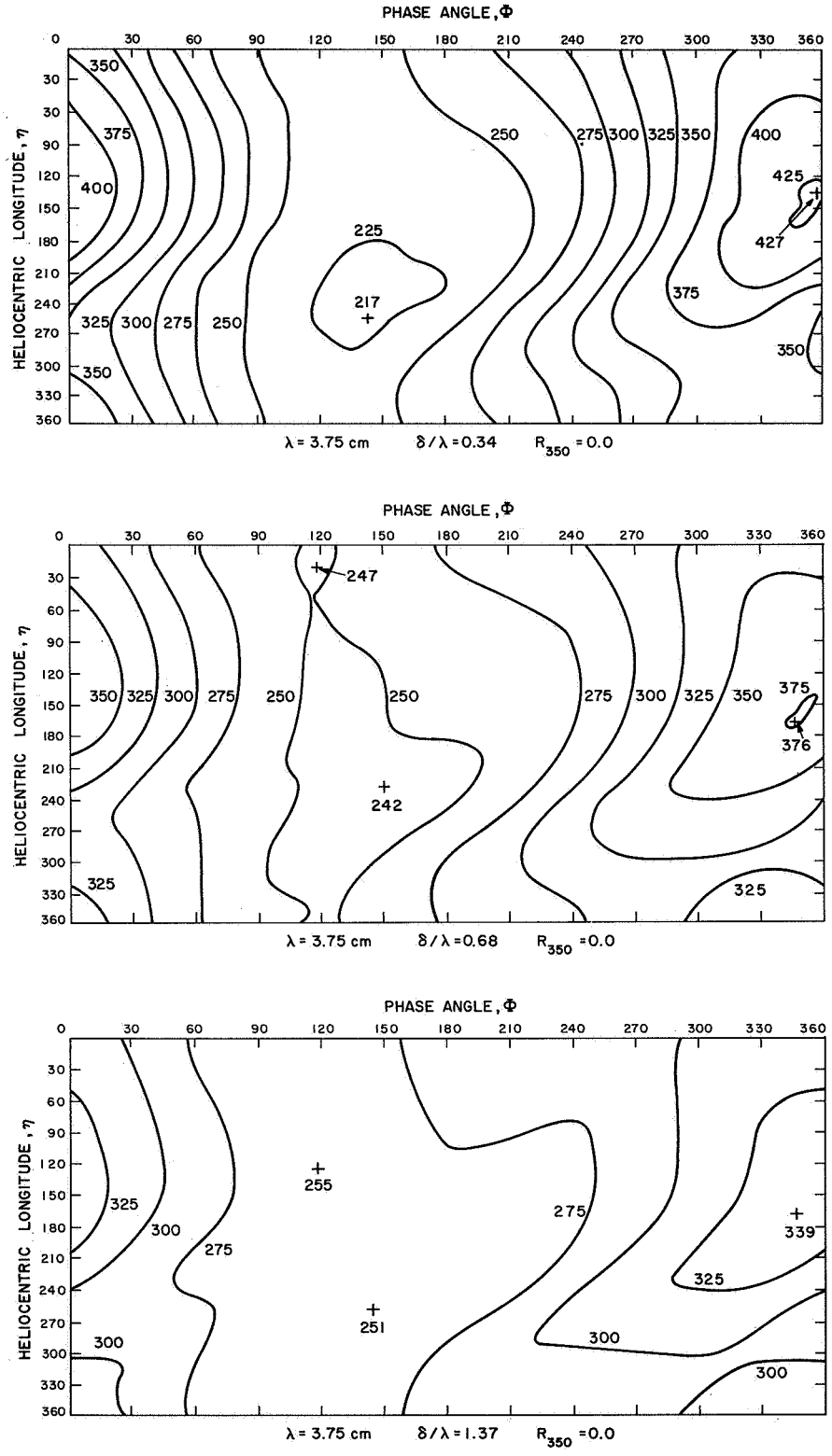

Figure 7. Computed brightness temperature as a function of Φ, η, and γ_{350} for $R_{350} = 0$ and $\lambda = 3.75$ cm.

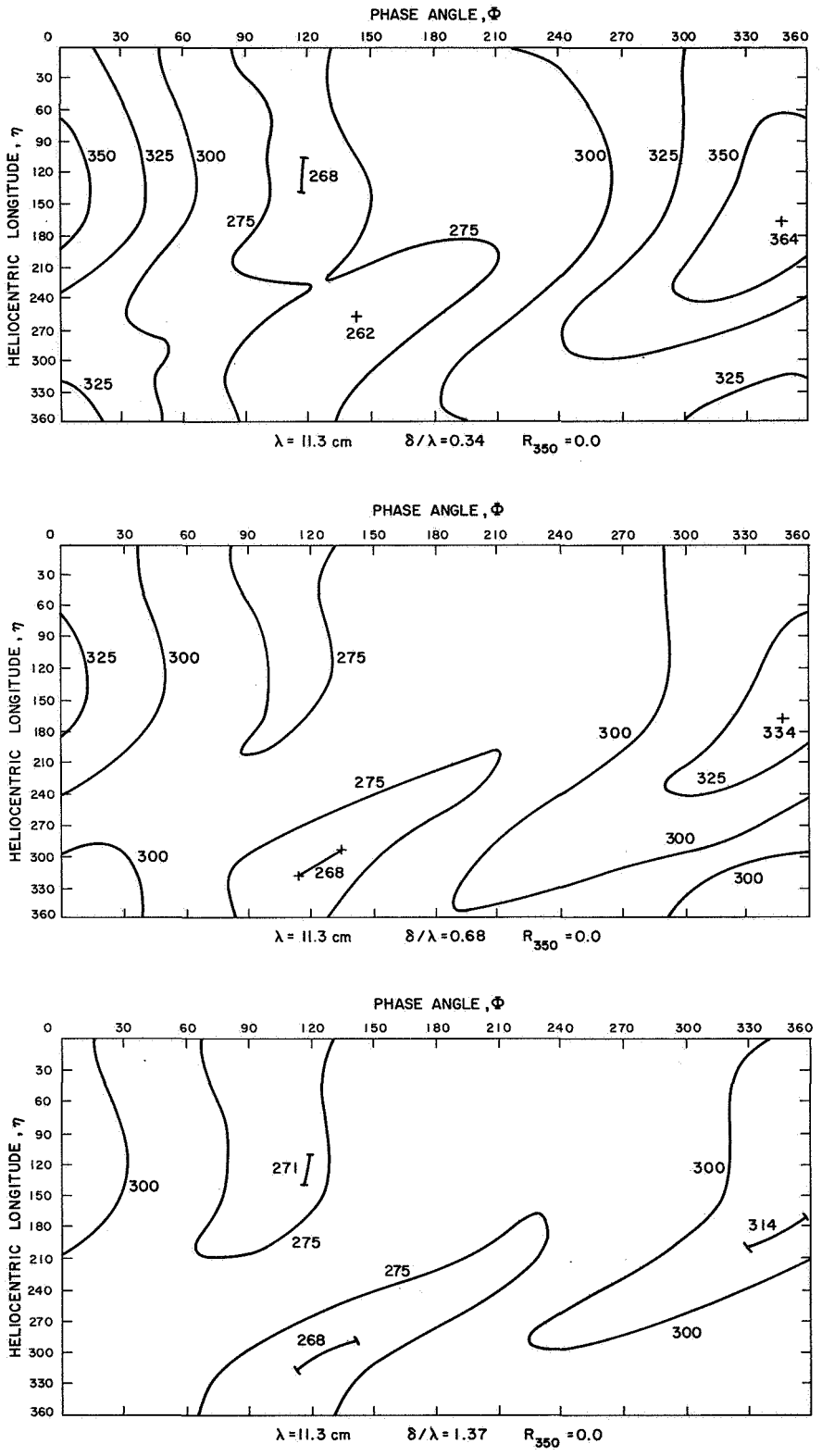

Figure 8. Computed brightness temperature as a function of Φ, η, and γ_{350} for $R_{350} = 0$ and $\lambda = 11.3$ cm.

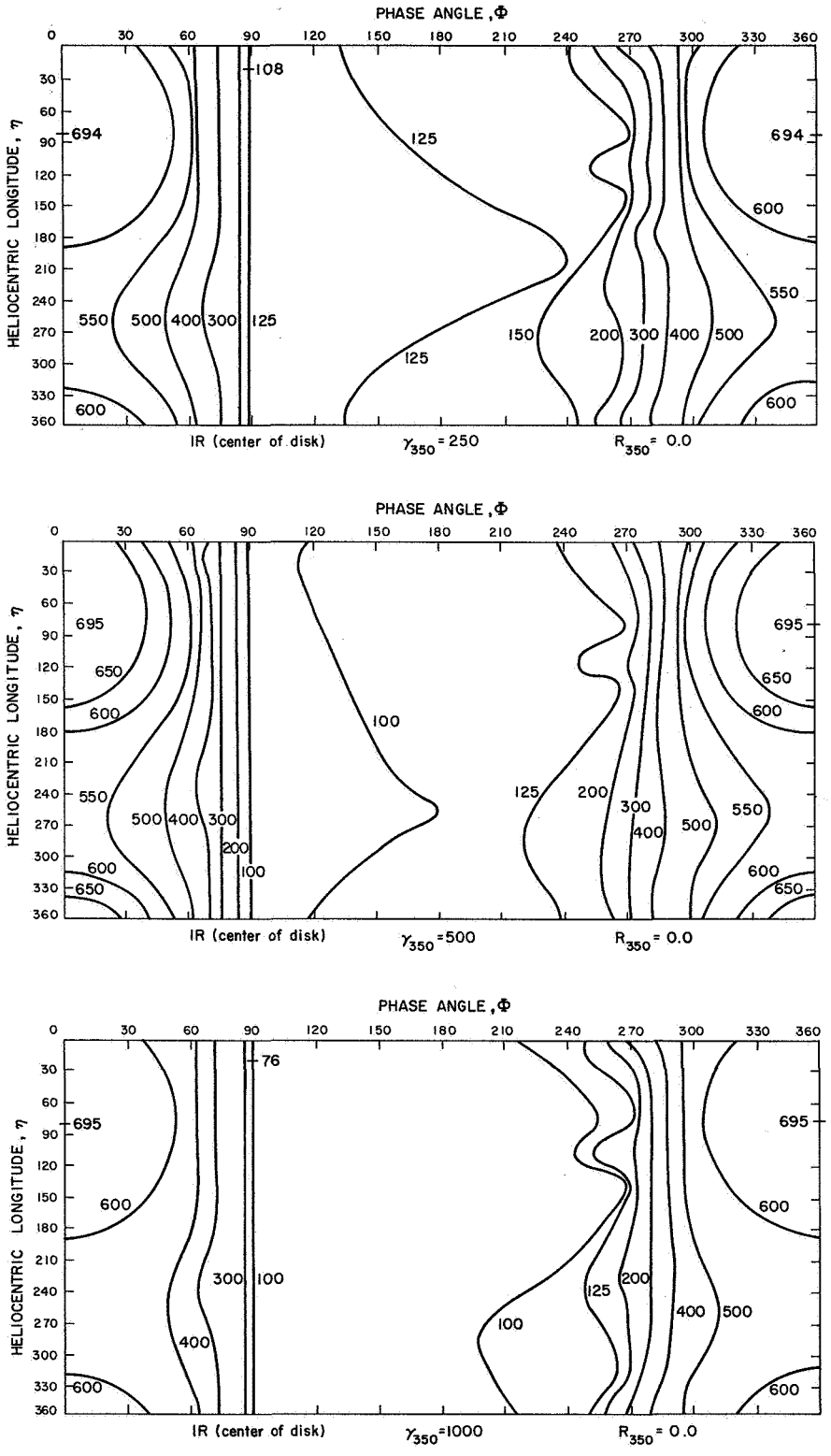

Figure 9. Center-of-disk infrared brightness temperature as a function of Φ and η for the indicated values of γ_{350} and R_{350}.

In order to obtain a particular phase curve from one of the contour plots, we use the phase angle Φ and heliocentric longitude η given as a function of date in the American Ephemeris. The path of the planet across the plot is then an irregular diagonal line from upper left to lower right, and the temperatures can be read directly as a function of time or of Φ from the intersections of this line with the temperature contours. In general, the phase curve for one apparition will differ from that for another. However, Klein (1968a) has pointed out that, because two solar days on Mercury are approximately equal to three synodic periods, at the end of three apparitions the (Φ,η) curve will very nearly repeat itself. Thus, even though we should not average data taken in successive synodic periods, it is usually satisfactory to average with data taken three synodic periods (or about one terrestrial year) earlier.

As we go from short to long wavelengths, the amplitude of the phase effect decreases, but even at very long wavelengths it never approaches zero. This is because with the 2:3 spin-orbit coupling, the heat budgets of different longitudes are permanently unequal. Thus, the equilibrium temperature at great depths will be higher at some longitudes than at others; with $\gamma_{350} = 500$ cal^{-1} cm^2 sec$^{1/2}$ deg and $R_{350} = 0.0$, this temperature varies from 269° to 345°K with a 90° change in planetary longitude. Let us consider the contour plots in Figure 8, where most of the diurnal temperature variation has been damped out. The peculiar shape of the contour lines in this figure can be understood if we follow one of the two longitudes for which the Sun is overhead at perihelion, at $\eta \cong 80°$. That point will be at the center of the disk as seen from Earth at $\Phi = 0°$, near the maximum temperature on the plot. After 44 days have passed and the planet is at aphelion with $\eta \cong 260°$, this point will have rotated $(-1/3) \times (360°)$ in phase angle, to about $\Phi = 240°$. We note that the temperature maximum follows just such a path in Figure 8. The characteristic zigzag shape of the contour lines is caused by the small apparent angular rotation of the planet with respect to the Sun (and hence to the Earth) near $\eta = 80°$. Here the contours run nearly vertical, while near $\eta = 240°$, when the apparent rotation is fastest, they have the smallest slope. In addition to the point of maximum temperature that we

have been following, there is a secondary maximum 180° away in planetary longitude and therefore also 180° away in phase.

4.2 Microwave Behavior with Constant Conductivity

To compare the predictions of these models with those of previous theories, we must consider the average variation of temperature as a function of phase angle alone. For this purpose, I have used the plots of Figures 3 to 8 to generate phase curves for the three apparitions of 1967. As an example, the 1967 temperatures at a wavelength of 1.90 cm are plotted in Figure 10. Asymmetries in the curves and variations in shape and amplitude from one apparition to the next are clearly present.

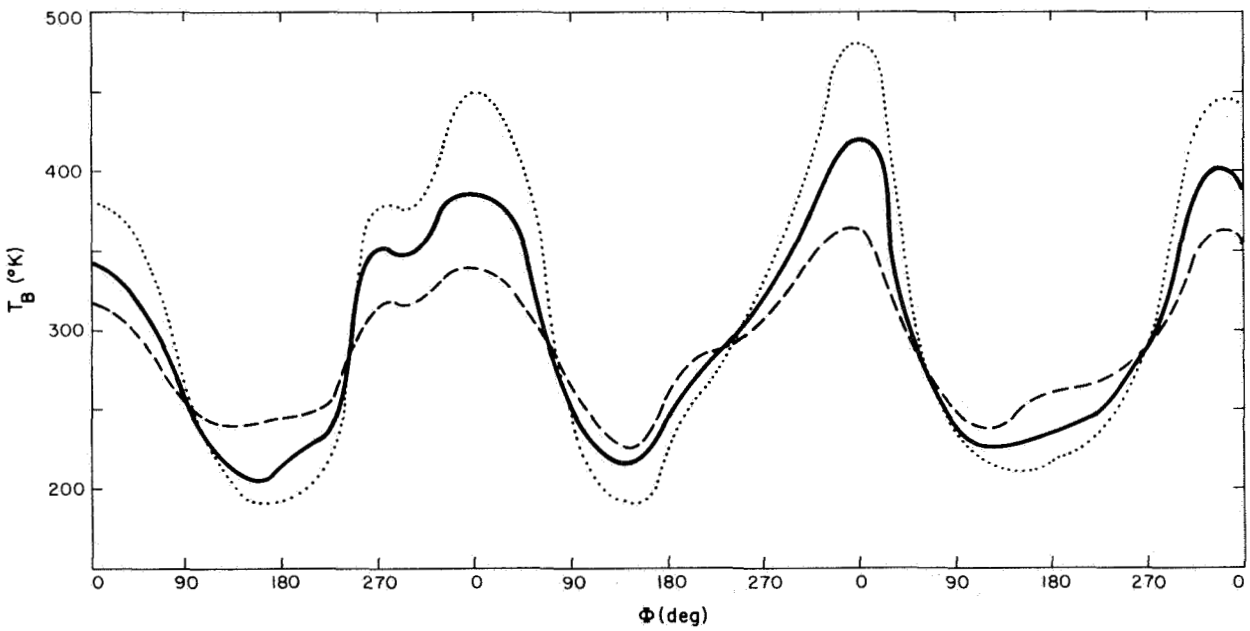

Figure 10. Model-predicted brightness temperatures at λ = 1.90 cm during 1967. The data are taken from Figure 6 for three values of γ_{350}.

A Fourier analysis of curves such as those in Figure 10 leads to a quantitative description of these variations. The temperature as a function of phase angle can be represented by the series

$$T(\Phi) = T_0 + \sum C_n \cos\left(\frac{n\pi\Phi}{1080} - \psi_n\right) \quad , \tag{20}$$

where the basic period is taken as three synodic periods, or 348 days, and the phase angle is in degrees. We can associate several of the harmonics with physically significant periods on Mercury. The main harmonic should be at the synodic period of 116 days. There will also be an effect due to varying distance from the Sun with a period of 88 days, and this will beat with 116 days to produce a variation with period about 350 days, as noted in the previous section. In addition, there is the effect of the permanently hotter and cooler planetary longitudes. A given longitude is at the center of the planet as seen from Earth at an average interval of 70 days, which is the reciprocal of the difference of the sidereal rotational frequency of Mercury and the orbital frequency of Earth. Thus, the average interval between hot longitudes is 35 days, and the beat of this with the synodic period is 50 days. Finally, we can expect a component at 58 days, the first overtone of the basic synodic period and hence the third coefficient in a Fourier series representation of the thermometric temperature variation at a point. We shall examine the phase and the amplitude for the 1967 predictions of the models for the Fourier components with these periods: 348, 116, 88, 58, 50, and 35 days.

The first term of the Fourier series, the mean temperature, depends on the choice of γ, since at the surface γ determines the rate of cooling at night; the larger is γ, the greater the insulation and the more rapid the cooling of the surface layers. In the absence of radiative conduction, the mean disk brightness temperature is independent of wavelength. For these 1967 curves, this temperature is 286°K at $\gamma = 1000$, 295°K at $\gamma = 500$, and 306°K at $\gamma = 250$ cal^{-1} cm^2 $sec^{1/2}$ deg.

The behavior of the most important harmonic, that with period 116 days, is illustrated in Figures 11 and 12. The amplitude, shown in Figure 11 as a percent of the mean temperature, decreases with wavelength, following a simple exponential decline at 2 cm and longer. These curves are in good agreement with those obtained by Gary (1967) from a scaling of solutions originally found for the Moon (Piddington and Minnett, 1949; Weaver, 1965). The phase lag (Figure 12) varies from a limit near -40° at long wavelengths to a value of about -5° in the far infrared. In the absence of any phase lag in the first harmonic of the surface temperature variation, the microwave phase lag predicted from this lunar theory should go from 0° to -45°.

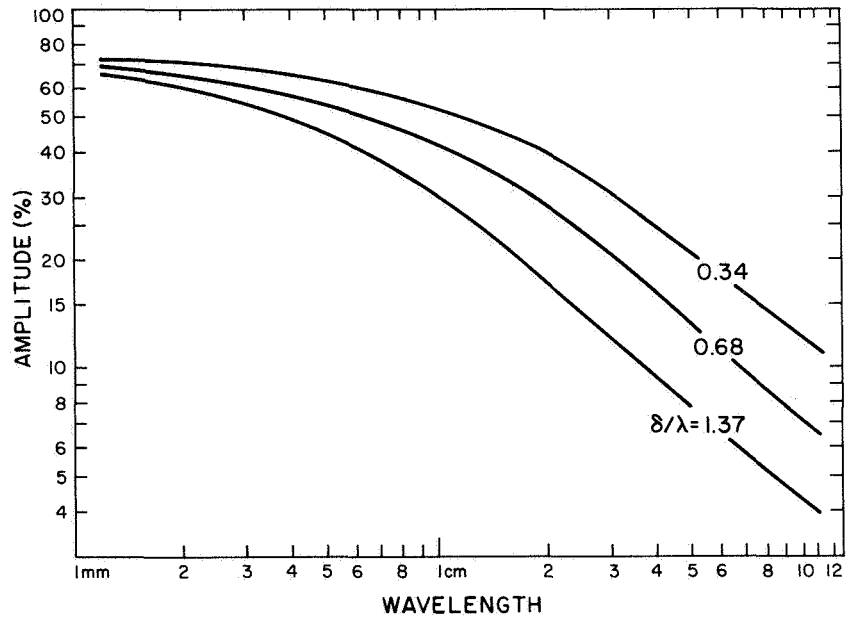

Figure 11. Amplitude of the phase effect (116-day period) as a function of wavelength obtained by Fourier analysis of the model predictions for 1967.

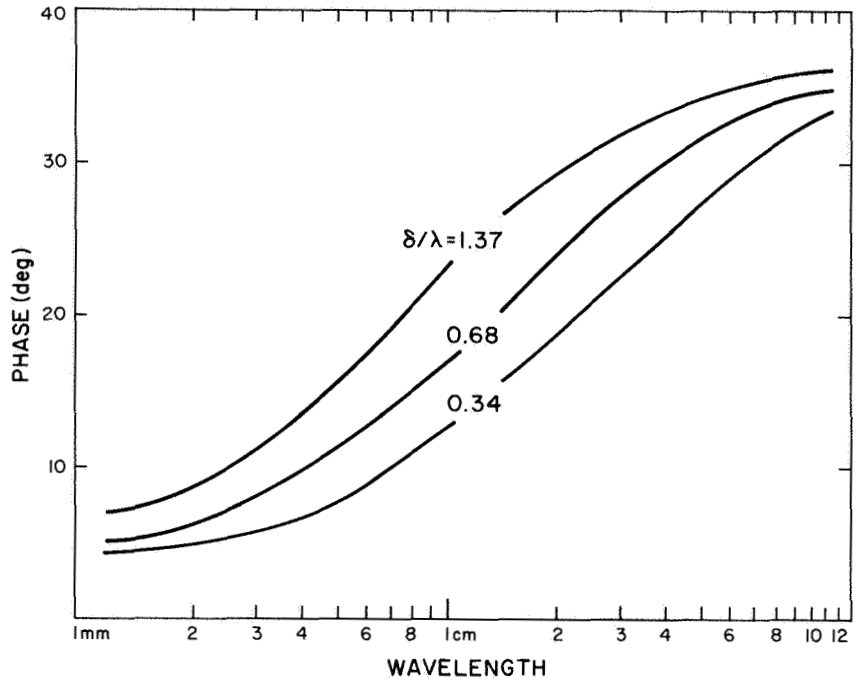

Figure 12. Phase lag of the phase effect (116-day period) as a function of wavelength obtained by Fourier analysis of the model predictions for 1967.

The first overtone of the synodic period is the second-most important Fourier component. The variation with wavelength follows closely the log-log plot given in Figure 11 for the 116-day component. For the model with $\gamma = 500$ (and therefore $\delta/\lambda = 0.68$ cm^{-1}), the amplitude varies from 9% at 1.2 mm to 2% at 11.3-cm wavelength. The phase lag is essentially zero for all wavelengths. The behavior of this overtone illustrates the rapid attenuation with depth of the higher order terms in the diurnal variation of surface temperature.

The components with an 88-day period and a 348-day period also show a parallel decrease in amplitude with wavelength, from about 5% to 1%. The phase lag at 88 days is 140° ± 10°; at 348 days, it is 170° ± 10°. The amplitude of the 35-day component is only 3% ± 1%, but it is approximately independent of wavelength, consistent with its origin in the permanent differences in temperature between hot and cool planetary longitudes. The beat of this term with the synodic period is the third-most important harmonic component, as

noted also by Klein (1968a) in his analysis of the 3.75-cm phase effect. It first increases with wavelength to a maximum of 7% at about 1 cm, then decreases to 2% at 11.3 cm.

This discussion confirms the presence of the harmonic components that are expected from a qualitative analysis of Mercury's orbit and rotation period. No other term in this Fourier analysis of the 1967 models has an amplitude greater than 2%.

4.3 Effects of Radiative Conductivity

When R_{350} is allowed to take nonzero values, the heat-conduction problem becomes nonlinear. In order to preserve zero net flux averaged over one diurnal cycle, the average subsurface temperature gradient must be higher at night than in the daytime; the result is to raise the mean temperature in the subsurface with respect to that on the surface. Thus, mean temperature increases with depth, approaching a fixed value several thermal wavelengths below the surface. Consider the equatorial temperatures at the hottest longitude. Figure 13 illustrates the variation of temperature with depth where $\gamma_{350} = 500$ cal^{-1} cm^2 sec$^{1/2}$ deg. The equilibrium temperature at great depth at this position is shown in Figure 14 as a function of R_{350} and γ_{350}. Observationally, these increased thermometric temperatures appear as an increase in mean brightness temperature with wavelength, approaching a maximum value as δ becomes much greater than unity. An increase of this sort has been reported for the Moon (see, e.g., Linsky, 1966; Troitsky, 1967; Troitsky et al., 1968).

While the shape of the phase curve for Mercury also changes from its constant conductivity form when $R_{350} \neq 0$, this change is small compared with the general increase in the brightness temperatures with increasing R_{350}. Figure 15 shows the mean brightness temperature as a function of wavelength and of R_{350} obtained from a Fourier analysis of the 1967 predictions with $\gamma_{350} = 500$ cal^{-1} cm^2 sec$^{1/2}$ deg. At wavelengths of 3.4 mm and shorter, the temperatures are not altered significantly. Beyond $\lambda = 11.3$ cm,

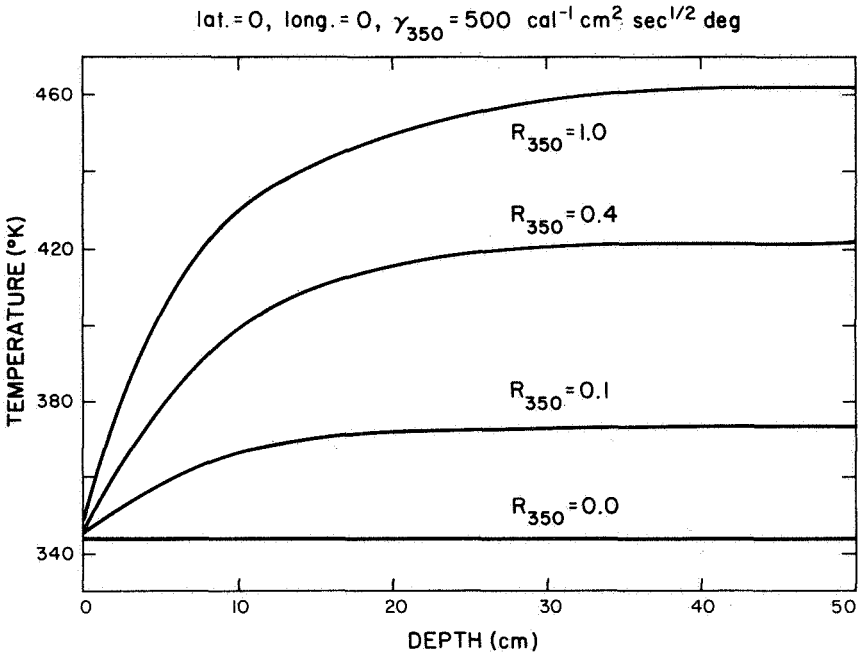

Figure 13. Equatorial thermometric mean temperature at a hot longitude as a function of depth below the surface for models having γ_{350} = 500 cal^{-1} cm^2 sec$^{1/2}$ deg and values of R_{350} from 0.0 to 1.0.

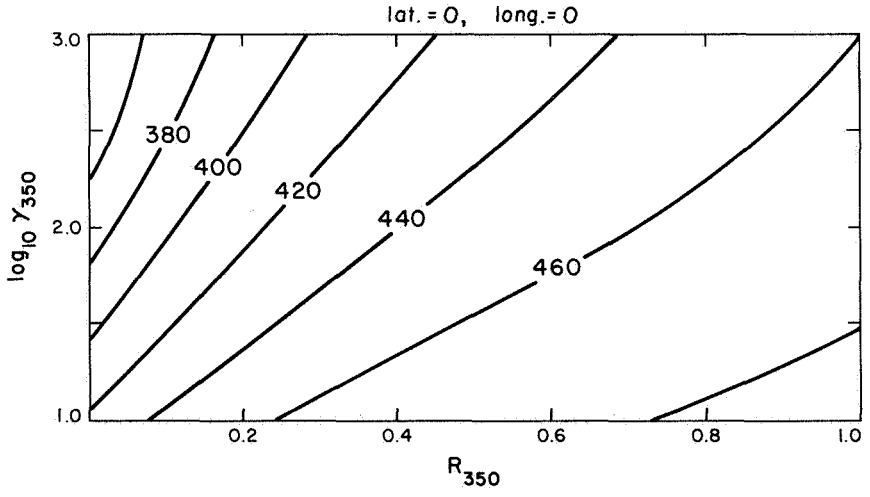

Figure 14. Equilibrium equatorial thermometric temperature at several thermal wavelengths below the surface at a hot longitude, given as a function of γ_{350} and R_{350}.

there is little further variation with wavelength. The temperature contour maps at $\lambda = 1.9$ cm and $\lambda = 3.75$ cm are illustrated in Figures 16 and 17 for a range of R_{350}.

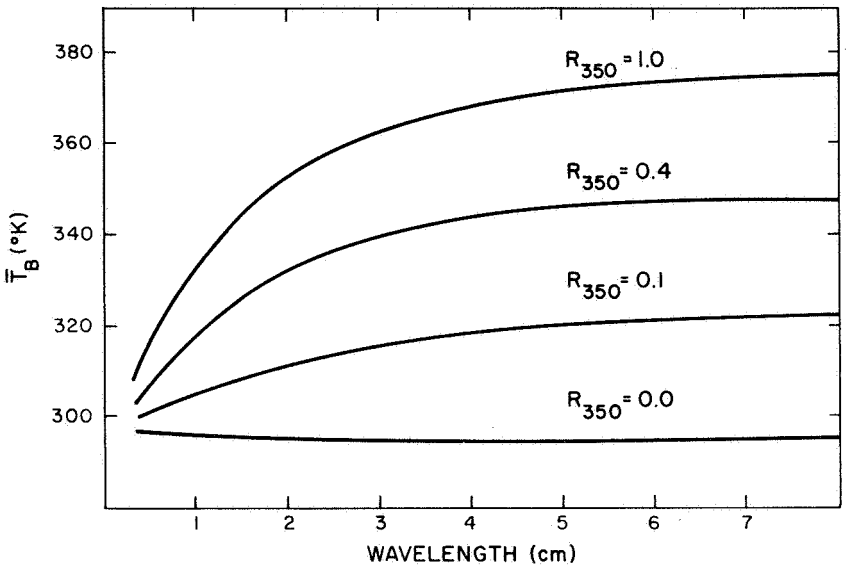

Figure 15. Mean radio brightness temperature as a function of λ and R_{350} for the 1967 predictions of models having $\gamma_{350} = 500$ cal^{-1} cm^2 sec$^{1/2}$ deg.

When the temperature-dependent conductivity is specified by $\gamma_{350} = 500$ cal^{-1} cm^2 sec$^{1/2}$ deg, as in the models of Figures 16 and 17, the amplitude of the 116-day phase variation is seen to increase somewhat as R_{350} increases. However, when the amplitude is expressed relative to the mean temperature, it is essentially independent of choice of R_{350}. Thus, we see that by evaluating the temperature-dependent conductivity at the temperature of 350°K, we can preserve the definition of thermal skin depth and of δ previously found with the assumption of constant thermal conductivity. In general, the phase curve obtained with a particular choice of γ_{350} and R_{350} can be very closely approximated by taking the curve computed with $R_{350} = 0$ and the same value of γ and multiplying all temperatures by the ratio indicated in Figure 15, thus extending the usefulness of the contour maps given in Figures 3-9.

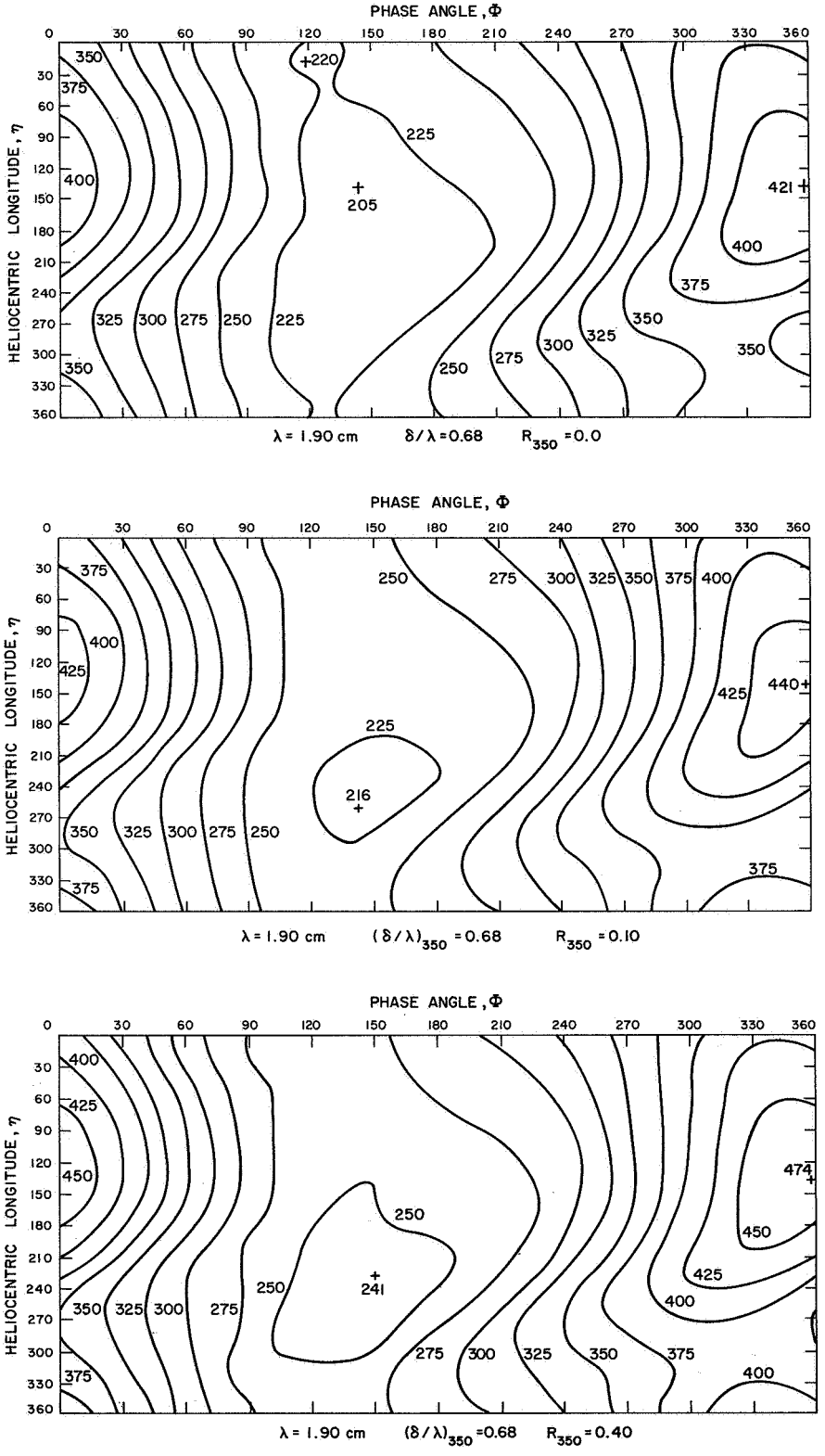

Figure 16. Computed brightness temperature as a function of Φ, η, and R_{350} for $\gamma_{350} = 500$ cal^{-1} cm^2 sec$^{1/2}$ deg and $\lambda = 1.90$ cm.

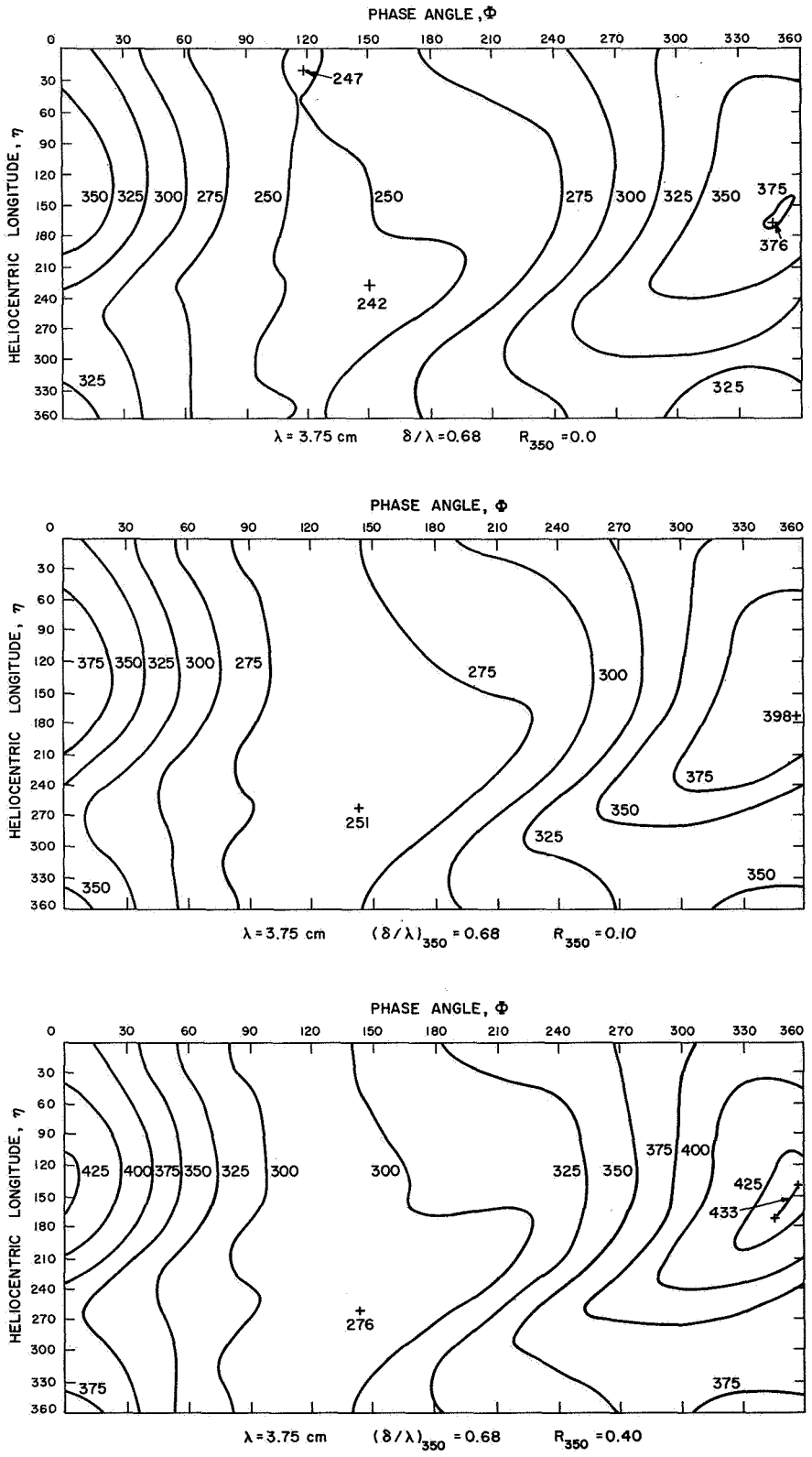

Figure 17. Computed brightness temperature as a function of Φ, η, and R_{350} for $\gamma_{350} = 500$ cal^{-1} cm^2 sec$^{1/2}$ deg and $\lambda = 3.75$ cm.

Depending on the radio observations available, either δ/λ (evaluated at $T = 350°K$) or R_{350}, or both, can be determined (within the assumptions of this discussion). In the usual case, the absolute calibration of a set of microwave observations has much more uncertainty than the relative temperatures that define the phase variation. It is then possible to use this phase variation, expressed in percent, to find δ/λ independent of both the absolute calibration and the degree of radiative conduction. Alternatively, if it is possible to make an observation with high absolute accuracy, then R_{350} can be found without observing other points on the phase curve, if δ/λ is known. If δ/λ is not known, R_{350} can still be determined from a single observation if it is made near greatest elongation of Mercury, where the phase curves for different values of δ/λ intersect.

5. COMPARISON WITH OBSERVATIONS

5.1 Infrared Observations

Observations of Mercury through the 8- to 14-μ atmospheric window have been made over half a century, but in only a very few cases has there been any resolution of the disk. When the entire disk is measured in the infrared, any flux from the dark side is unmeasurable in comparison with the high flux from the hotter regions. Since the higher temperatures represent near-equilibrium with the local insolation, the large infrared fluxes are not dependent on subsurface conduction. Only observations made of resolved parts of the night side of Mercury, uncontaminated by daytime fluxes, are useful in determining the thermal properties of the epilith.

On June 21, 1923, Pettit and Nicholson (1923) obtained an uncalibrated thermocouple reading of the 8- to 14-μ radiation from part of the unilluminated disk of Mercury. This observation has recently been discussed by Soter (1966), who used an energy calibration from later observations by Pettit and Nicholson (1936) and deduced a lower limit on the mean night-side temperature at the time of the observation of 180°K. Using Soter's description of the circumstances of the observation, I have reduced these data without the necessity of his retrospective calibration. Pettit and Nicholson obtained readings on an arbitrary scale from both the illuminated and the unilluminated parts of the planet in their 1923 observation. In the illuminated crescent, the surface is in approximate equilibrium with the insolation, so that the temperatures are independent of the assumed thermal model but are dependent only on the orbital configurations of Mercury and the Earth. For the phase angle $\Phi = 247°$ and heliocentric longitude $\eta = 316°$, I have calculated, from the thermal models presented in this report, the distribution of temperature across the disk; the equatorial temperatures are illustrated in Figure 18. After integrating the flux from the planet over the observing aperture and

correcting for background reading from the sky, I find that the observed deflections imply an infrared specific intensity from the night side of between 2% and 4% of the bright-side value, depending on the positioning of the radiometer aperture. When the flux in the 8- to 14-μ window from the bright side is calculated from the model, the dark-side flux is found to imply a temperature of 180° to 200°K, in agreement with the reduction by Soter (1966). As is clear from Figure 18, a temperature as high as 180°K is not compatible with any value of the thermal parameter given here but implies $\gamma < 100$ cal^{-1} cm^{2} sec$^{1/2}$ deg. However, the usefulness of this observation is questionable. In their 1936 paper summarizing all their previous Mercury observations, Pettit and Nicholson gave only data obtained for the whole disk and specifically stated that measurements of the dark-side temperature cannot be made (cf. Belton et al., 1967).

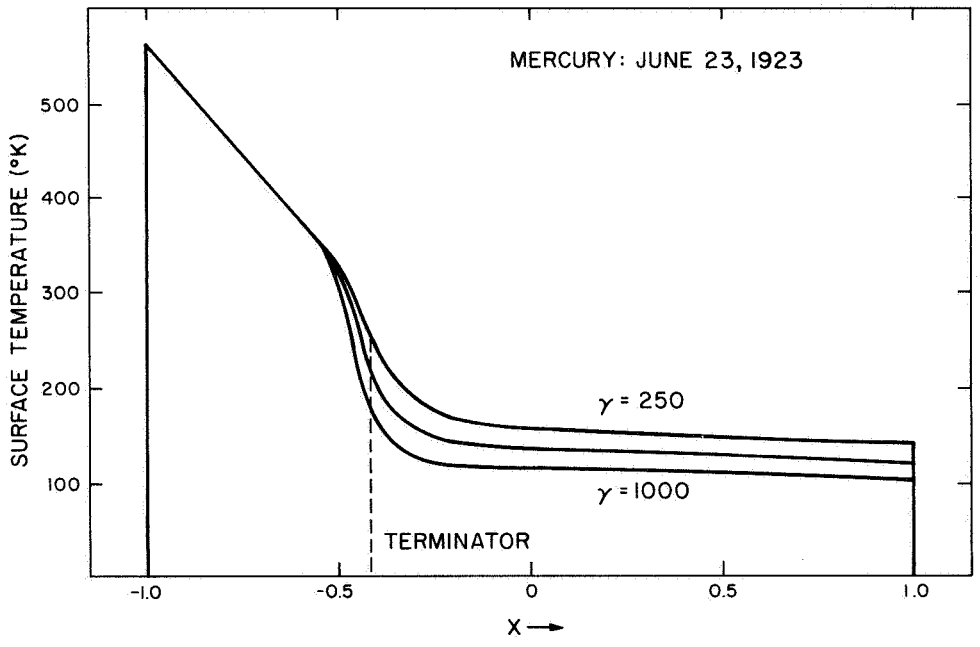

Figure 18. Distribution of equatorial surface temperature across the disk of Mercury on June 21, 1923, as calculated from the models.

A recent observation of Mercury in the 8- to 14-μ band has been reported by Murray (1967), who used higher angular resolution and greater sensitivity than were available to Pettit and Nicholson. He estimates an upper limit to the midnight equatorial temperature of 150°K. He thus fails to detect a flux that is less than one fifth as large as that reported by Pettit and Nicholson, and this contradiction cannot be attributed to the orbital geometry of Mercury, since the night temperatures are only very weakly dependent on planetary longitude (see Figure 9). Murray's observation requires that $\gamma > 200$ cal^{-1} cm^2 sec$^{1/2}$ deg.

5.2 Observations at 3.4 mm

Observations at this wavelength have been made during the past several years by Epstein and his coworkers with the 4.6-m telescope of the Aerospace Corporation. In an early report (Epstein, 1966), no phase effect was indicated, but with an improved signal-to-noise ratio and a longer observing baseline, a variation with phase was found (Epstein, Soter, Oliver, Schorn, and Wilson, 1967). A least-squares fit of a cosine wave to the data from two synodic periods in 1966 gave the following parameters:

$$T_B = (291 \pm 15) + (87 \pm 18) \cos [\Phi + (41 \pm 13)]°K.$$

A similar fit to the combined 1965 and 1966 data gave essentially the same result. A comparison of the amplitude of this phase effect (30 ± 5%) with Figure 11 and with the calculations of Gary (1967) yields a value of $3 < \delta/\lambda < 4$ for the ratio of skin depths divided by the wavelength. Gary correctly noted that this result was not consistent with the value of δ/λ determined from observations at 1.9 cm (discussed below).

For direct comparison with the models presented here, I have separated the data given by Epstein et al. (1967) that were obtained in different apparitions and have recomputed normal points. In Figure 19, these points with their standard deviations are compared with predictions from the models with $\delta/\lambda = 0.34$, 0.68, and 1.36 cm^{-1}. In spite of the small amplitude

derived from the least-squares fit of a cosine curve to these data, the 1966 points appear to be compatible with these computed curves. The 1965 points, however, are clearly not internally consistent. We shall therefore concentrate on the 1966 data alone.

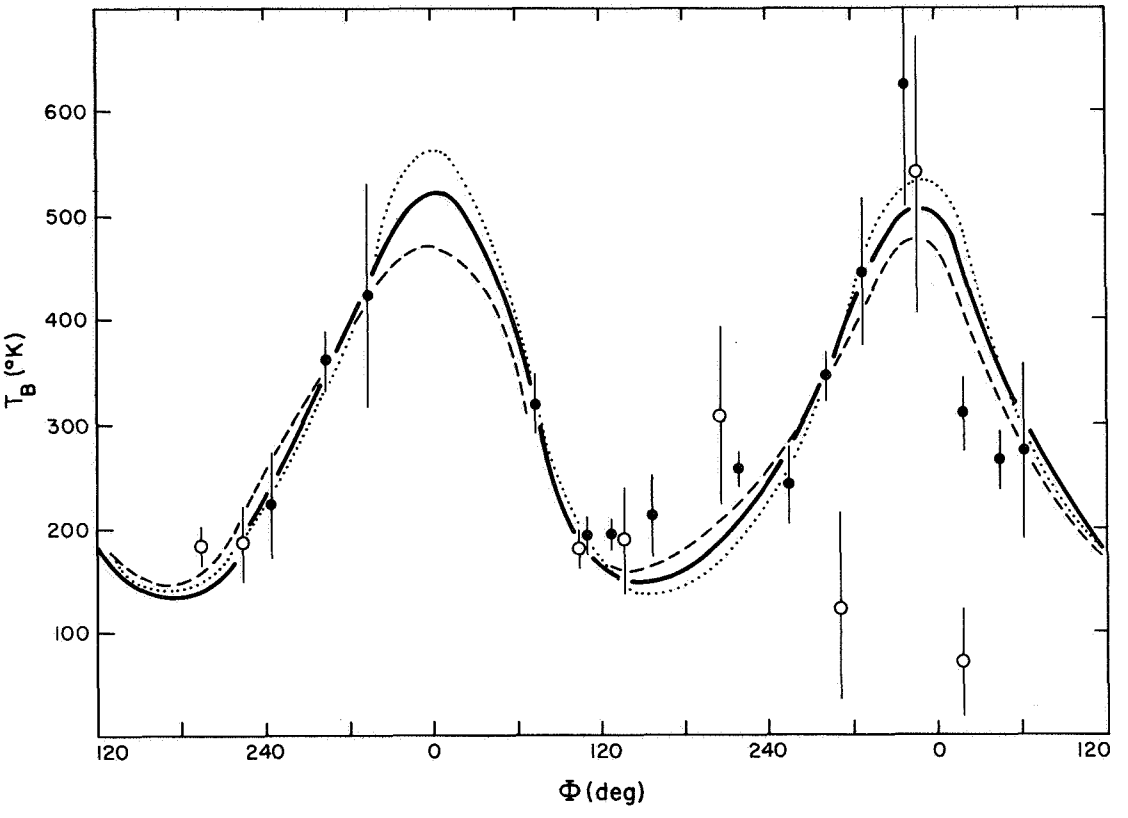

Figure 19. Observed brightness temperatures at $\lambda = 3.4$ mm (Epstein et al., 1967) compared with predictions of models having $\delta/\lambda = 0.34$ (dotted), $\delta/\lambda = 0.68$ (solid), and $\delta/\lambda = 1.36$ cm^{-1} (dashed). Closed circles are 1966 data, and open circles are 1965 data. Errors indicated are the standard deviation on the mean for each normal point.

Before we conclude which models are really inconsistent with these data, it is useful to consider the meaning of the formal uncertainties obtained from the curve-fitting process, such as the ±18°K given by Epstein et al. (1967) for the amplitude of the phase variation. Each of these uncertainties is computed on the assumption that the other two variables of the three-parameter cosine fit are held fixed at their correct values. Let us consider,

however, fitting a curve to periodic data in which the values around one phase are much better determined than elsewhere along the curve. It is unrealistic in such a case to treat the variation in the three parameters independently. For instance, good fits can be obtained for a wide range of amplitudes if the mean value is simultaneously adjusted to ensure that the fitted curve continues to pass through the well-determined points. This suggests the danger of relying too much on the formal uncertainties in the parameters when a curve is fitted to data with nonuniform spacing.

As an illustration of the problem discussed above, I have obtained least-squares fits of a number of periodic functions to the 1966 Mercury observations. Of the 101 points given by Epstein et al. (1967), 4 were excluded as obviously inconsistent and the remaining 97 were each given equal weight. The best-fitting cosine curve is

$$T_B = 284 + 102 \cos (\Phi + 27)^\circ K \quad ,$$

in fair agreement with the weighted fit given by Epstein. The rms deviation of the data points from this curve, defined as the square root of the average of the residuals squared, is 96°K. If, however, the amplitude is held fixed and a best fit is obtained by adjusting only the mean temperature and phase lag, the results shown in Figure 20 are obtained. Here, both the mean temperature and the rms deviation of the data from the curve are plotted as functions of the amplitude, expressed as a percent of the mean temperature. There is little variation in phase lag among these fits. Also shown in this figure are results of fitting two phase curves derived from the models having $R_{350} = 0.0$ and $\delta/\lambda = 0.68$ and $1.36\ cm^{-1}$. The fitting was accomplished by adjusting the scales to allow for possible errors in absolute calibration of the observations or for the influence of a radiative term in the conductivity, as discussed in Section 4.3. This one-parameter fit of the models gives essentially the same rms deviation as the two-parameter fits of cosine waves having the same amplitude. It appears not only that these data are incapable of discriminating between the model predictions and simple cosine curves, but also that the best-fitting cosine curve is only marginally superior in fit to any

other curve in the amplitude range $15\% < \Delta T < 55\%$. Thus, any value of δ/λ between 1.0 and 8.0 cm^{-1} is probably compatible with the observations. Temperatures computed from models having $\gamma = 250$ or 500 $cal^{-1}\ cm^2\ sec^{1/2}$ deg fit the data best when they are lowered by 5% to 10%; however, the temperatures obtained with $\gamma = 1000$ require no adjustment. This result could be interpreted as indicating the larger value of γ; however, the absolute calibration of these observations is uncertain by 5% to 10%, so that in practice no conclusions about the size of γ can be drawn.

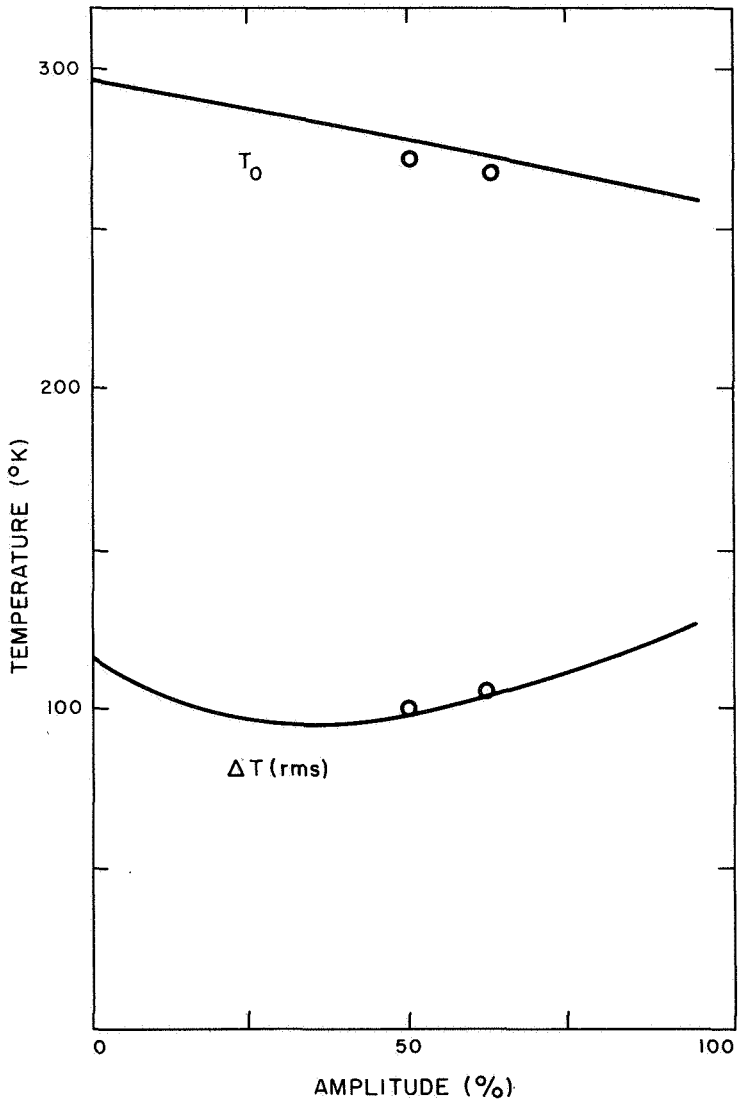

Figure 20. Fits of cosine curves to the 1966 data at $\lambda = 3.4$ mm. The mean temperature and rms deviation of the points from the cosine curves are shown as functions of the amplitude of the curves. The two open circles are computed from model phase curves (see text).

5.3 Observations at 8.0 mm

Observations of a phase effect at 8-mm wavelength have been reported recently by Golovkov and Losovskii (1968). The measurements were made with the 22-m telescope of the Lebedev Institute of Physics, USSR, in May to July 1966. Venus and Jupiter were used as calibration standards. The least-squares cosine fit to their 10 observed temperatures is given as

$$T_B = (530 \pm 50) + (290 \pm 70) \cos [\Phi + (0 \pm 15)]^\circ K$$

It is immediately obvious that these temperatures are implausibly high, since near superior conjunction the disk-averaged brightness temperature exceeds by more than 100° the maximum equatorial surface temperature possible on Mercury. If, however, we use these results from Golovkov and Losovsky in spite of the apparent calibration error of nearly a factor of 2, we find that the amplitude of 55% implies a value of $\delta/\lambda = 0.40$ cm^{-1}. Because of the calibration error, however, this result is of dubious value and will not be used in later discussions in this report.

5.4 Observations at 1.94 cm

The microwave observations of Mercury having the highest signal-to-noise ratio were made by Kaftan-Kassim and Kellermann (1967) with the 43-m telescope of the National Radio Astronomy Observatory in Green Bank, West Virginia, at a wavelength of 1.94 cm. They obtained 11 temperature points in February and March 1966, covering phase angles from 40° to 200°. Calibration sources were Virgo A, Hydra A, 3C161, Venus, Jupiter, and Saturn. A fit of a cosine curve to the weighted data points gives

$$T_B = (288 \pm 7) + (75 \pm 13) \cos [\Phi + (38 \pm 17)]^\circ K \quad .$$

The absolute calibration uncertainty is thought to be no more than 15%, with the above values probably a few percent too low (K. I. Kellermann, 1968, private communication). From this amplitude of 26% ± 6%, Figure 11 gives $\delta/\lambda = 0.80\ (+0.40, -0.25)$ cm^{-1}.

A direct comparison of the observations with the models is shown in Figure 21. From inspection of the curves, it appears that the data are compatible with $0.6 < \delta/\lambda < 1.30$, in agreement with the value quoted above from comparison with the average amplitude predicted for 1967. None of the curves is a very impressive match to the data, however. The rms deviation of the data from the model curves is slightly larger than the deviation from the best-fitting cosine curve, but of course the cosine curve is adjusted through three parameters to fit these particular data points, while the model curves vary in only one parameter, δ/λ. The mean value of 288°K is in agreement with the models having $R_{350} = 0.0$ and $\gamma_{350} = 500$ cal^{-1} cm^2 sec$^{1/2}$ deg, as is also clear from the comparison of models and data points shown in Figure 21.

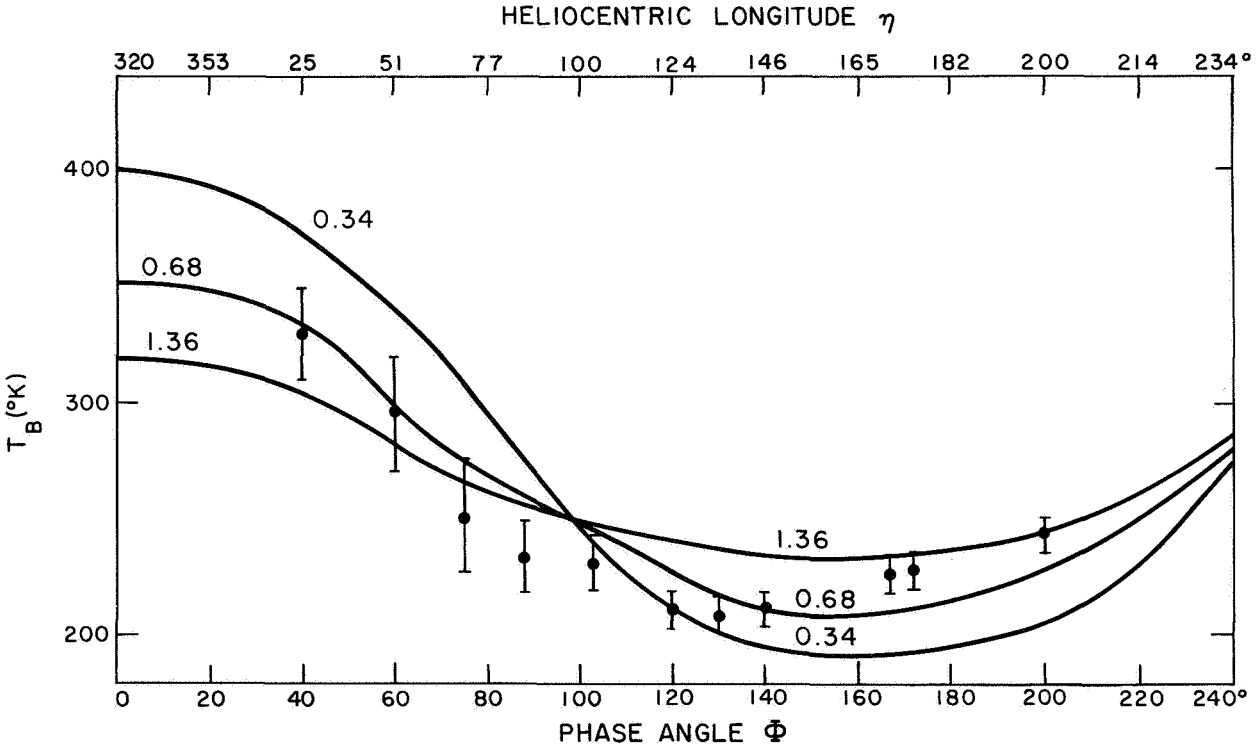

Figure 21. Observations at $\lambda = 1.9$ cm compared with model predictions for $R_{350} = 0.0$ and $\delta/\lambda = 0.34$, 0.68, and 1.36 cm^{-1}. The data points with their error bars are taken from Kaftan-Kassim and Kellermann (1967).

My own observations of Mercury at this wavelength were made partly by use of the same telescope and general observing techniques employed by Kaftan-Kassim and Kellermann (1967) and partly by use of the 37-m telescope of the MIT-Lincoln Laboratory Haystack Microwave Facility.* The temperatures were determined in each case by direct comparison with Venus, assumed to have a brightness temperature of 485 (+60, -40)°K (Morrison, 1969). The observed temperatures are consistently higher than those measured by Kaftan-Kassim and Kellermann, although their calibration was based in part on a brightness temperature of 500°K for Venus. The observations are plotted in Figure 21. The apparent absence of a variation with phase suggests that $\delta/\lambda > 1.0$ cm^{-1}. The two curves plotted in Figure 22 were computed with $\delta/\lambda = 1.36$ cm^{-1} and with R_{350} equal to zero (bottom curve) and 0.4 (top curve). The fit with the top curve is satisfactory, although with so few observations these results must be treated with caution.

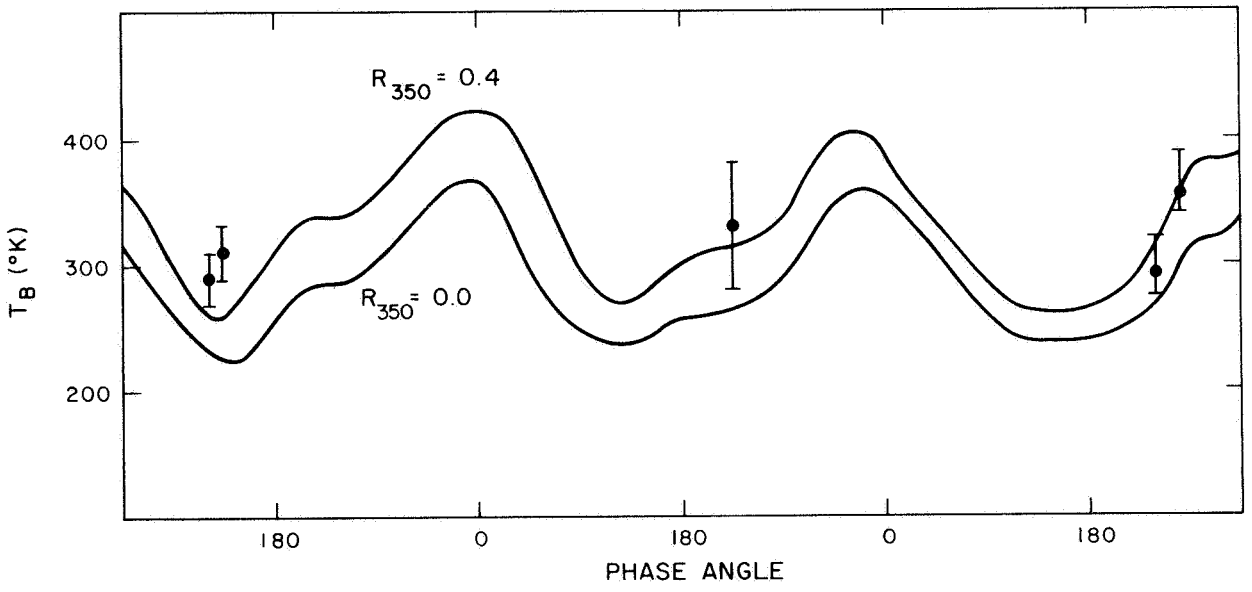

Figure 22. Observations at $\lambda = 1.94$ cm made by Morrison in June 1967, November 1967, February 1968, and March 1968. The model curves illustrated are computed with $\delta/\lambda = 1.36$ cm^{-1} ($\gamma_{350} = 1000$) and R_{350} equal to 0 and to 0.4.

*A full description of these observations will be published elsewhere.

5.5 Observations at 2.82 cm

A single measurement of Mercury made at 2.82-cm wavelength with the 46-m telescope of the National Research Council of Canada has kindly been communicated to me by W. J. Medd (1968, private communication). The temperature near elongation ($\Phi = 105°$) was $350° \pm 18°$ K (internal rms error). This temperature is $80° \pm 40°$ K higher than is predicted by the models with $R_{350} = 0.0$, thus supporting the suggestion of an increase in mean brightness temperature of Mercury with wavelength.

5.6 Observations at 3.75 cm

The most extensive set of microwave observations of Mercury yet made has recently been completed by M. J. Klein, who used the 28-m telescope of the University of Michigan to observe over seven synodic periods at a wavelength of 3.75 cm. Klein (1968a, b) has made a direct comparison of his data with previously published models (Morrison and Sagan, 1967) and has also (1968b) compared the data with five-parameter curves that include a variation of temperature with hermocentric longitude (35-day period) as well as with phase (116-day period). The best-fitting such curve is

$$T_B = (355 \pm 4) + (51 \pm 3) \cos [\Phi + (32 \pm 4)] + (10 \pm 1) \cos [2\ell - (8 \pm 11)]°K \quad ,$$

where ℓ is the hermocentric longitude. The phase-effect amplitude of 14% corresponds (from Figure 11) to $\delta/\lambda = 0.9$ cm^{-1}, and the phase lag of 32° gives (from Figure 12) the same result. The amplitude of the second cosine coefficient of 3% agrees with the amplitude of this term derived in Section 4.2 for all wavelengths. The observations and the best-fitting curve are plotted in Figure 23, taken from Klein (1968b). The plot and the curve fitting are both made on the assumption that the brightness curve is approximately periodic with period 350 days, or three synodic periods, as discussed in Section 4.1.

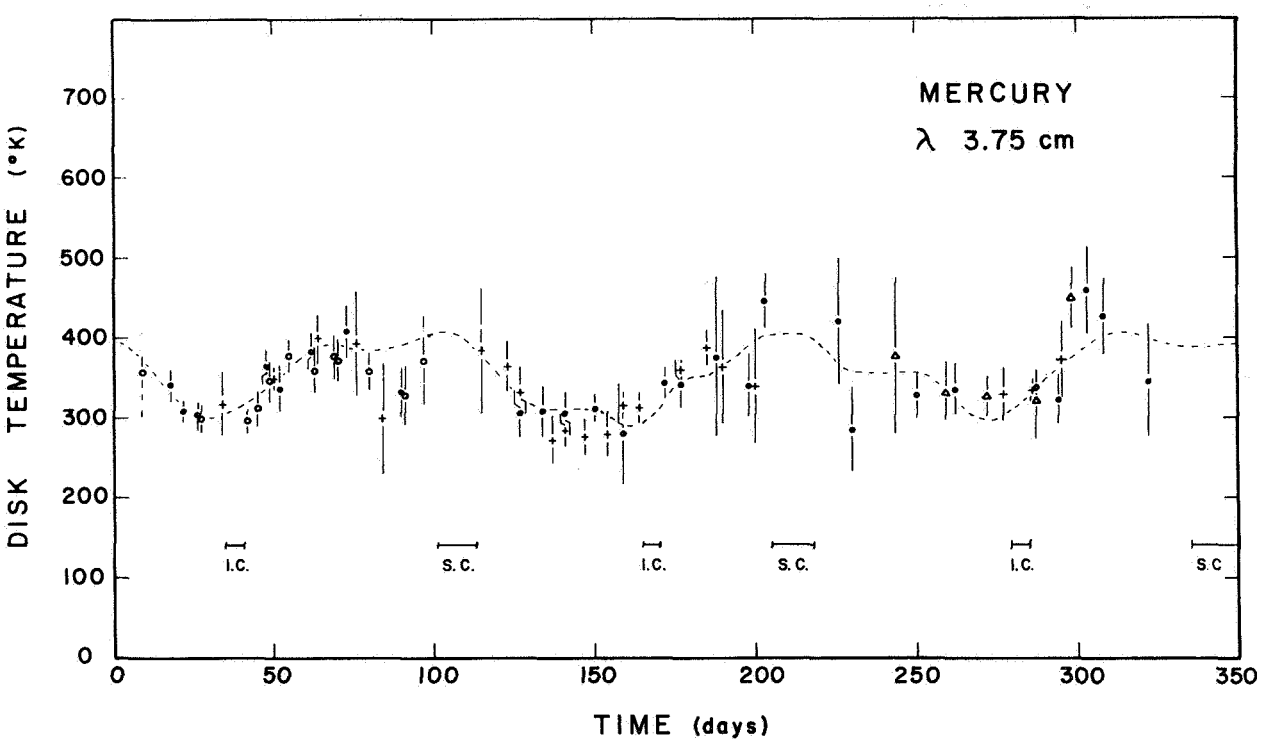

Figure 23. Observations at $\lambda = 3.75$ cm. The dashed curve is a best fit to the data (see text). This figure is taken from Klein (1968b).

From a direct comparison with the models (Morrison and Sagan, 1967), Klein gives $0.68 < \delta/\lambda < 1.36$ cm^{-1}; this agrees with the value of δ/λ determined from the fitted amplitude and phase lag of the phase effect. The observations, when compared with models having $R_{350} = 0.0$, are systematically high by about 20%; this is also clear from the mean temperature of 355°K quoted above.

These observations at 3.75 cm are the only ones published to date with a high-enough signal-to-noise ratio and a long-enough time base to demonstrate a dependence of brightness temperature on longitude for Mercury. When sufficient observations are available at any wavelength, the curve-fitting approach used by Klein should prove very useful. In most cases, however, the data are insufficient and more information can be derived by a comparison with two-parameter models as discussed in this report.

5.7 Observations at 11.3 cm

Using the 64-m telescope of the Commonwealth Scientific and Industrial Research Organization at Parks, Australia, in the spring of 1964, Kellermann (1965, 1966) made a series of observations at this wavelength, covering phase angles from 30° to 125°. Hydra A was used as a calibration standard. The mean brightness temperature was about 300°K, and no substantive phase effect was found. An approximate upper limit of about 100° can be set on the amplitude of the phase variation, indicating $\delta/\lambda > 0.15$ cm^{-1}. From a point-by-point comparison with the phase curve from Figure 8 for $\delta/\lambda = 0.68$ cm^{-1}, I find that the systematic deviation of the observations from the curves is $-2° \pm 14°$K. Thus, these observations do not confirm the increase of brightness temperature with wavelength discussed in the preceding sections.

6. CONCLUSIONS

In this report, I have discussed the computation of infrared and microwave brightness temperatures for the planet Mercury from direct computer calculations of thermal conduction and radiation processes in the planetary epilith. This analysis is considerably more involved than those given previously (Gary, 1967; Belton et al., 1967), in which solutions obtained for the thermal behavior of the Moon are simply scaled to Mercury's mean solar distance and rotation rate. There are, however, two important advantages in these numerical models: they illustrate the dependence of temperature on the orbital position of the planet, and they allow a treatment of temperature-dependent thermal conductivity. In Section 4, I have examined the differences between the predictions of these models and those obtained from the lunar scaling, and in Section 5, I have compared the predictions with the data. Most of the observations are of insufficient accuracy to require the numerical theory for their interpretation, but the observations at wavelengths of 1.94 and 3.75 cm do begin to show orbital and radiative effects, and we can expect that in the future even better observational material will be available.

From the amplitude and shape of the phase variation of microwave brightness temperature, the parameter δ/λ has been determined at several wavelengths. In Figure 24, these results are summarized. Relying primarily on the observations at 1.94 and 3.75 cm, I derive a most probable value for δ/λ of 1.0 cm^{-1}, with likely upper and lower limits of 1.5 and 0.7 cm^{-1}. For comparison with other planets, I use the product of δ/λ and the square root of the mean solar period; this parameter, which is independent of solar period, is therefore descriptive of the physical nature of the subsurface material (see Pollack and Sagan, 1965; Morrison and Sagan, 1967). If the unit of time is the mean solar year, the value of this parameter for Mercury is 0.7 ± 0.3 cm^{-1} $yr^{1/2}$, in good agreement with a value for the Moon of 0.9 cm^{-1} $yr^{1/2}$ (Gary, 1967) to 0.6 cm^{-1} $yr^{1/2}$ (Clardy and Straiton, 1968). These results are not in agreement with those of Golovkov and

Losovskii (1968), who conclude from their analysis of microwave observations of Mercury that $\delta/\lambda \simeq 0.1$ cm^{-1} and hence that the subsurface materials of Mercury and the Moon are distinctly different. However, these authors use neither the known range of surface temperature on Mercury nor the recent observations of Klein (1968b) in their analysis, so that their results are subject to large uncertainties.

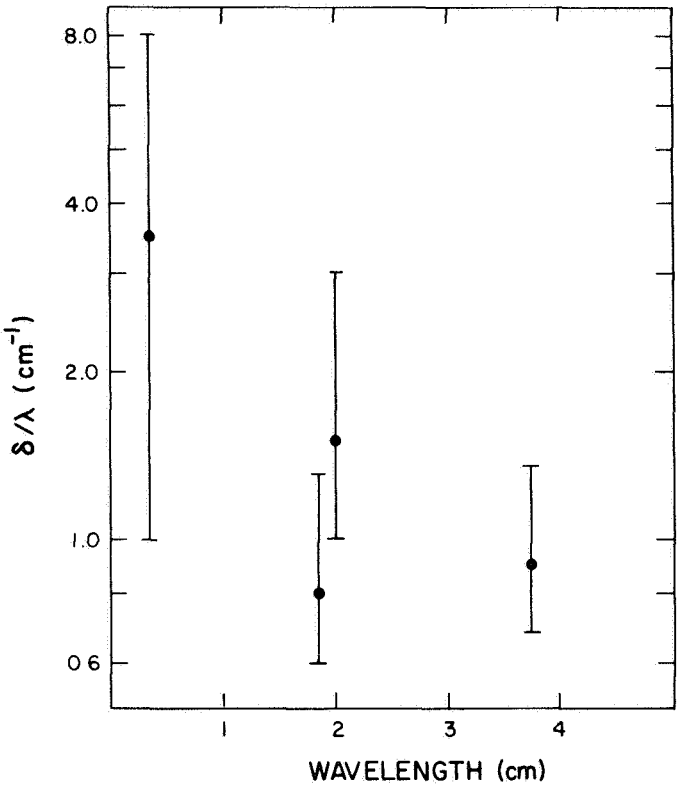

Figure 24. Summary of the observational determination of δ/λ (cm^{-1}) for Mercury.

From the upper limit to the night infrared temperature given by Murray (1967), we can estimate that the thermal parameter γ_{350} is greater than 200 cal^{-1} cm^{2} sec$^{1/2}$ deg. In accepting this, we must disregard the contradictory observation made in 1923 by Pettit and Nicholson. Under the assumptions that most of the conductivity at this temperature is supplied by contact conduction and not by radiation and that $\rho c = 0.30$ cal cm^{-3} deg^{-1}, the thermal conductivity is

$$K_0 < 10^{-4} \text{ cal cm}^{-1} \text{ sec}^{-1} \text{ deg}^{-1} \quad .$$

For comparison, the lunar conductivity is of the order of 10^{-5} and that of terrestrial rocks is 10^{-3} or more in the same units. The thermal skin depth can be computed from the conductivity as follows:

$$L_t = \left(\frac{K_0 P}{\pi \rho c}\right)^{1/2} \text{ cm} \quad , \tag{21}$$

where P is the length of the day. Evaluating this expression, we find $L_t < 40$ cm.

Using both the thermal skin depth and the value of δ/λ determined above, we can investigate the electrical properties of the epilith. From equation (16), the electrical skin depth is less than 40 λ, and k_0, the microwave absorption cross section multiplied by the wavelength, is greater than 0.04. This is consistent with the lunar value for k_0 of 0.1. The loss tangent can be found from k_0 and from the index of refraction of 1.7 determined from the radar cross section of Mercury: $\tan \Delta > 2 \times 10^{-3}$. All these inequalities could be changed to equalities if the night-side infrared temperature of Mercury were measured; this is the crucial observation from which the thermal conductivity in the epilith can be found.

The variation of mean brightness temperature with wavelength is diagnostic of the significance of temperature-dependent conductivity on Mercury. In Figure 25, the mean temperatures from the observations are compared with the model predictions illustrated in Figure 15. The data are clearly contradictory, with a sizable increase of temperature above the $R_{350} = 0.0$ model indicated by the observations of Morrison, Medd, and Klein, but with no increase found by Kaftin-Kassim and Kellermann, or by Kellermann? These differences cannot be explained as due to different calibration systems; all observers used values for the standard sources in near agreement with the recent flux scale suggested by Scheuer and Williams (1968), and all used the American Ephemeris value for the radius of Mercury [which has recently been confirmed by direct radar measurement (Ash, Shapiro, and Smith, 1967)].

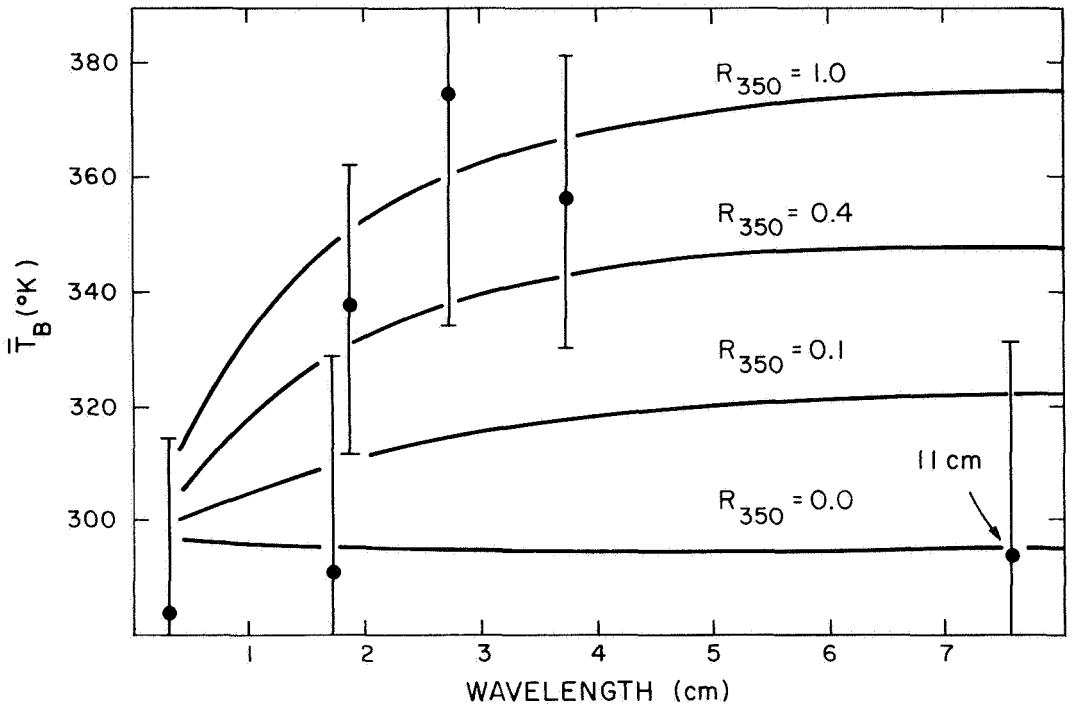

Figure 25. Mean microwave brightness temperatures as determined from the observations, compared with the curves of Figure 15.

In spite of the contradictions, the data plotted in Figure 25 do strongly suggest an increase of brightness temperature with wavelength, and I suggest a tentative value of $R_{350} = 0.5$. This can be compared with a value of R_{350} near unity suggested for the Moon by Linsky (1966) from an analysis similar to that presented here. The difference between these two values is probably not significant. If $R_{350} = 0.5$, then the coefficient B of equation (6) is about 10^{-8} times the contact conductivity K_0. We estimated above that $K_0 < 10^{-4}$, so that $B < 10^{-12}$. From equations (18) and (19), we can estimate the mean free path of a thermal photon for this range of B, remembering that $\sigma = 1.35 \times 10^{-12}$ in these units; we find that this length must be less than 2 mm. For the more probable value of $K_0 = 10^{-5}$, this distance is reduced to 200 μ. Even if it is established that R_{350} is smaller for Mercury than for the Moon, this does not necessarily imply that particles

are smaller or more compacted on Mercury; it may be the result, at least in part, of a somewhat greater contact conductivity on Mercury than on the Moon. More observations are needed to clarify the situation.

Although the physical properties, such as thermal conductivity, loss tangent, and particle size, are not determined with as much accuracy as we might wish from the available data, still it is clear that the epilith of Mercury is not composed of solid, compact rock. All the evidence presented here, as well as the results of photometric and polarimetric studies, supports the hypothesis that the epilith of Mercury is very similar to that of the Moon.

7. ACKNOWLEDGMENTS

I wish to express my gratitude to Carl Sagan, James B. Pollack, and Nancy D. Morrison for their assistance and encouragement. I have also profited by discussions with Eugene Epstein, K. I. Kellermann, M. J. Klein, Jeffrey Linsky, Richard Munro, and Joseph Veverka. I am grateful to M. J. Klein and W. J. Medd for communicating their results in advance of publication, and to M. J. Campbell and S. L. Soter for critically reading the manuscript.

REFERENCES

ASH, M. E., SHAPIRO, I. I., and SMITH, W. B.

1967. Astronomical constants and planetary ephemerides deduced from radar and optical observations. Astron. Journ., vol. 72, pp. 338-350.

BELTON, M. J. S., HUNTEN, D. M., and McELROY, M. B.

1967. A search for an atmosphere on Mercury. Astrophys. Journ., vol. 150, pp. 1111-1124.

BERGSTRALH, J. T., GRAY, L. D., and SMITH, H. J.

1967. An upper limit for atmospheric carbon dioxide on Mercury. Astrophys. Journ., vol. 149, pp. L137-L139.

CAMICHEL, H., and DOLLFUS, A.

1968. La rotation et la cartographie de la planète Mercure. Icarus, vol. 8, pp. 216-226.

CAMPBELL, M. J., ULRICHS, J., and GOLD, T.

1968. Density of the lunar surface. Science, vol. 159, p. 973.

CHAPMAN, C. R.

1967. Optical evidence on the rotation of Mercury. Earth Planet. Sci. Lett., vol. 3, pp. 381-385.

CHRISTENSEN, E. M., BATTERSON, S. A., BENSON, H. E., CHAOTE, R., JAFFE, L. D., JONES, R. H., KO, H. Y., SPENCER, R. L., SPERLING, F. B., and SUTTON, G. H.

1968. Lunar surface mechanical properties at the landing site of Surveyor 3. Journ. Geophys. Res., vol. 73, pp. 4081-4094.

CLARDY, D. E., and STRAITON, A. W.

1968. Radiometric measurements of the Moon at 8.6- and 3.2-millimeter wavelengths. Astrophys. Journ., vol. 154, pp. 775-782.

COLOMBO, G.

1965. Rotational period of the planet Mercury. Nature, vol. 208, p. 575.

COLOMBO, G., and SHAPIRO, I. I.

1966. The rotation of the planet Mercury. Astrophys. Journ., vol. 145, pp. 296-307.

CRUIKSHANK, D. P., and CHAPMAN, C. R.

1967. Mercury's rotation and visual observations. Sky and Tel., vol. 34, pp. 24-26.

DE VAUCOULEURS, G.

1964. Geometric and photometric parameters of the terrestrial planets. Icarus, vol. 3, pp. 187-235.

DYCE, R. B., PETTENGILL, G. H., and SHAPIRO, I. I.

1967. Radar determination of the rotations of Venus and Mercury. Astron. Journ., vol. 72, pp. 351-359.

EPSTEIN, E. E.

1966. Mercury: Anomalous absence from the 3.4-millimeter radio emission of variation with phase. Science, vol. 151, pp. 445-447.

EPSTEIN, E. E., SOTER, S. L., OLIVER, J. P., SCHORN, R. A., and WILSON, W. J.

1967. Mercury: Observations of the 3.4-millimeter radio emission. Science, vol. 157, pp. 1550-1552.

GARY, B.

1967. Mercury's microwave phase effect. Astrophys. Journ., vol. 149, pp. L141-L145.

GOLDREICH, P., and PEALE, S. J.

1968. The dynamics of planetary rotations. Ann. Rev. Astron. Astrophys., vol. 6, pp. 287-320.

GOLOVKOV, V. K., and LOSOVSKII, B. Ya.

1968. Measurements of the phase dependence of the 0.8-cm radio emission of Mercury, and some properties of its surface layer. Soviet Astron.-A. J., vol. 12, pp. 299-302.

HARRIS, D. L.

1961. Photometry and colorimetry of planets and satellites. In Planets and Satellites, edited by G. P. Kuiper and B. M. Middlehurst, University of Chicago Press, Chicago, pp. 272-342.

HOVIS, W. A., and CALLAHAN, W. R.

1966. Infrared reflectance spectra of igneous rocks, tuffs, and red sandstone from 0.5 to 22 μ. Journ. Opt. Soc. Amer., vol. 56, pp. 639-643.

HOWARD, W. E., III, BARRETT, A. H., and HADDOCK, F. T.

1962. Measurement of microwave radiation from the planet Mercury. Astrophys. Journ., vol. 136, pp. 995-1004.

JAEGER, J. C.

1953. The surface temperature of the Moon. Austral. Journ. Phys., vol. 6, pp. 10-21.

JAFFE, L. D., BATTERSON, S. A., BROWN, W. E., JR., CHRISTENSEN, E. M., GAULT, D. E., LUCAS, J. W., NORTON, R. H., SCOTT, R. F., SHOEMAKER, E. M., SUTTON, G. H., and TURKEVICH, A. L.

1968. Principal scientific results of the Surveyor 3 mission. Journ. Geophys. Res., vol. 73, pp. 3983-3987.

JOHNSON, D. L.

1968. Lunar soil: Should this term be used? Science, vol. 160, p. 1258.

KAFTAN-KASSIM, M. A., and KELLERMANN, K. I.

1967. Measurements of the 1.9-cm thermal radio emission from Mercury. Nature, vol. 213, pp. 272-273.

KELLERMANN, K. I.

1965. 11-cm observations of the temperature of Mercury. Nature, vol. 205, pp. 1091-1092.

1966. The thermal radio emission from Mercury, Venus, Mars, Saturn, and Uranus. Icarus, vol. 5, pp. 478-490.

KLEIN, M. J.

1968a. Measurements of the 8-GHz phase effect of Mercury during seven synodic periods (abstract). Astron. Journ., vol. 73, p. S102.

1968b. The planet Mercury: Measurements of variations in the microwave disk temperature. Thesis, Univ. of Michigan, Ann Arbor, Michigan.

LINSKY, J. L.

1966. Models of the lunar surface including temperature-dependent thermal properties. Icarus, vol. 5, pp. 606-634.

LIU, H.-S., and O'KEEFE, J. A.

1965. Theory of rotation for the planet Mercury. Science, vol. 150, p. 1717.

MacDONALD, G. J. F.

1963. The deep structure of continents. Rev. Geophys., vol. 1, pp. 587-665.

McGOVERN, W. E., GROSS, S. H., and RASOOL, S. I.

1965. Rotation period of the planet Mercury. Nature, vol. 208, p. 375.

MORRISON, D.

1968a. On the interpretation of Mercury observations at wavelengths of 3.4 and 19 mm. Astrophys. Journ., vol. 152, pp. 661-664.

1968b. Martian surface temperatures. Smithsonian Astrophys. Obs. Spec. Rep. No. 284, 26 pp.

1969. Venus: Absence of a phase effect at 2 cm wavelength. Science, in press.

MORRISON, D., and SAGAN, C.

1967. The microwave phase effect of Mercury. Astrophys. Journ., vol. 150, pp. 1105-1110.

1968. Interpretation of the microwave phase effect of Mercury (abstract). Astron. Journ., vol. 73, pp. S27-S28.

MUNCEY, R. W.

1958. Calculations of lunar temperatures. Nature, vol. 181, pp. 1458-1459.

1963. Properties of the lunar surface as revealed by thermal radiation. Austral. Journ. Phys., vol. 16, pp. 24-31.

MUNRO, R.

1964. The determination of the properties and structure of the lunar surface through the phenomenon of temperature change. Jet Propulsion Lab. Space Program Summary, vol. 6, pp. 186-190.

MURRAY, B. C.

1967. Infrared radiation from the daytime and nighttime surfaces of Mercury (abstract). Trans. Amer. Geophys. Union, vol. 48, p. 148.

PEALE, S. J., and GOLD, T.

1965. Rotation of the planet Mercury. Nature, vol. 206, pp. 1240-1241.

PETTENGILL, G.

1965. Lunar radar reflections. In Solar System Radio Astronomy, edited by J. Aarons, Plenum Press, New York, pp. 355-369.

PETTENGILL, G. H., and DYCE, R. B.

1965. A radar determination of the rotation of the planet Mercury. Nature, vol. 206, p. 1240.

PETTENGILL, G. H., DYCE, R. B., and CAMPBELL, D. B.

1967. Radar measurements at 70 cm of Venus and Mercury. Astron. Journ., vol. 72, pp. 330-337.

PETTIT, E., and NICHOLSON, S. B.

1923. Measurements of the radiation from the planet Mercury. Publ. Astron. Soc. Pacific, vol. 35, pp. 194-198.

1936. Radiation from the planet Mercury. Astrophys. Journ., vol. 83, pp. 84-102.

PIDDINGTON, J. H., and MINNETT, H. C.

1949. Microwave thermal radiation from the Moon. Austral. Journ. Sci. Res., ser. A, vol. 2, pp. 63-77.

POLLACK, J. B., and SAGAN, C.

1965. The microwave phase effect of Venus. Icarus, vol. 4, pp. 62-103.

SAGAN, C.

1966. The photometric properties of Mercury. Astrophys. Journ., vol. 144, pp. 1218-1221.

SCHEUER, P. A. G., and WILLIAMS, P. J. S.

1968. Radio spectra. Ann. Rev. Astron. Astrophys., vol. 6, pp. 321-350.

SCOTT, R. F., and ROBERSON, F. I.

1968. Soil mechanics surface sampler: Lunar surface tests, results, and analyses. Journ. Geophys. Res., vol. 73, pp. 4045-4080.

SINTON, W.

1967. On the composition of Martian surface materials. Icarus, vol. 6, pp. 222-228.

SMITH, B. A., and REESE, E. J.

1968. Mercury's rotation period: Photographic confirmation. Science, vol. 162, pp. 1275-1277.

SOTER, S. L.

1966. Mercury: Infrared evidence for nonsynchronous rotation. Science, vol. 153, pp. 1112-1113.

SOTER, S. L., and ULRICHS, J.

1967. Rotation and heating of the planet Mercury. Nature, vol. 214, pp. 1315-1316.

TROITSKY, V.

1967. Thermal conductivity of lunite as dependent on temperature. Nature, vol. 213, pp. 688-689.

TROITSKY, V. S., BUROV, A. B., and ALYOSHINA, T. N.

1968. Influence of the temperature dependence of lunar material properties on the spectrum of the Moon's radio emission. Icarus, vol. 8, pp. 423-433.

VETUCHNOVSKAYA, Ya. N., and KUZMIN, A. D.

1967. The thermal radioemission of Mercury. Lebedev Institute of Physics, Radioastron. Lab. Preprint No. 153, 12 pp.

WALKER, J.C.G.

1961. The thermal budget of the planet Mercury. Astrophys. Journ., vol. 133, pp. 274-280.

WEAVER, H.

1965. The interpretation of thermal emission from the Moon. In Solar System Radio Astronomy, edited by J. Aarons, Plenum Press, New York, pp. 295-354.

WESSELINK, A. J.

1948. Heat conductivity and the nature of the lunar surface material. Bull. Astron. Inst. Netherlands, vol. 10, pp. 351-363.

BIOGRAPHICAL NOTE

DAVID MORRISON received the B.A. degree from the University of Illinois in 1962 and the M.A. degree from Harvard University in 1964.

Mr. Morrison is currently a Ph. D. degree candidate at Harvard University holding a Smithsonian Graduate Research Fellowship. He has previously been employed at the Smithsonian Astrophysical Observatory, the Jet Propulsion Laboratory, and the Naval Research Laboratory.

Mr. Morrison's principal research interests are in planetary physics, especially the measurement and interpretation of microwave radio temperatures of the terrestrial planets.

NOTICE

This series of Special Reports was instituted under the supervision of Dr. F. L. Whipple, Director of the Astrophysical Observatory of the Smithsonian Institution, shortly after the launching of the first artificial earth satellite on October 4, 1957. Contributions come from the Staff of the Observatory.

First issued to ensure the immediate dissemination of data for satellite tracking, the reports have continued to provide a rapid distribution of catalogs of satellite observations, orbital information, and preliminary results of data analyses prior to formal publication in the appropriate journals. The Reports are also used extensively for the rapid publication of preliminary or special results in other fields of astrophysics.

The Reports are regularly distributed to all institutions participating in the U. S. space research program and to individual scientists who request them from the Publications Division, Distribution Section, Smithsonian Astrophysical Observatory, Cambridge, Massachusetts 02138.